Journal of Sustainable Development of Energy, Water and Environment Systems

http://www.sdewes.org/jsdewes

Year 2026, Volume 14, Issue 2, 1140671

Original Research Article

Optimal Sizing PV- Battery Storage Fuel Cell Based Space Microgrids

***Khaled Wahdan*[*1], *Magda I. Ibrahim*[1], *Mohamed Elgamal*[2], *Abdelfattah A. Eladl*[2]**

[1] CEE Engineering Dept. Nile Higher Institute for Engineering and Technology, Mansoura, Egypt

[2] Electrical Engineering Department Faculty of Engineering, Mansoura University, El-Mansoura 35516, Egypt

e-mail: eladle7@mans.edu.eg, khaledwahdan36@gmail.com, Magdaebraheem15@gmail.com, engineer_elgamal@mans.edu.eg

Cite as: Wahdan, K., Ibrahim, M., Elgamal, M., Eladl, A. A., Optimal Sizing PV- Battery Storage Fuel Cell Based Space Microgrids, J.sustain. dev. energy water environ. syst., 14(2), 1140671, 2026, DOI: https://doi.org/10.13044/j.sdewes.d14.0671

ABSTRACT

This paper presents a techno-economic analysis and optimal sizing of a hybrid microgrid for a lunar surface base, combining a photovoltaic power system, a battery energy storage system, an electrolyzer, a hydrogen storage tank, and a hydrogen fuel cell. The components are coordinated by an energy management strategy that first supplies the load directly from solar power, then charges the battery, and finally produces and stores hydrogen for use by the fuel cell during power shortages. An hourly simulation model is developed using a representative lunar base load profile and environmental conditions consistent with space operation. The influence of photovoltaic capacity and battery technology is examined for three battery types: lithium-ion, lead–acid, and nickel–cadmium. For each case, a complete economic evaluation is performed, including capital, operation and maintenance, fuel, and replacement costs, together with system-level indicators of energy cost and storage cost. In addition, a mass-based assessment relates subsystem sizing to launch mass and transportation cost, which are critical for space missions. The results identify combinations of photovoltaic capacity and battery type that minimise energy cost while satisfying reliability requirements for a crewed lunar base, and they provide design guidelines for efficient hybrid microgrids in space applications.

KEYWORDS

Levelized cost of energy, Renewable energy sources, Hybrid systems in space, Lunar power system, Solar power in space, Space exploration.

INTRODUCTION

Starting in 2024, space agencies including NASA, JAXA, and CNSA aim to send missions to the Moon to create places for humans to live, with targeted timelines of 2030, and 2036, respectively [1]. Sherwood [2] outlined key principles for designing and operating a practical lunar base. Chavy-Macdonald *et al.* [3] developed a systems model for the cis-lunar resource ecosystem and explore scenarios for lunar resource industries and their broader impacts. Viterale [4] analyzed the systemic transition to a new space age in the 21st century and highlights the strategic role of lunar activities in that transition. Saha et al. [5] reviewed space microgrids for future manned lunar bases and emphasize the central importance of dedicated electrical power infrastructure. Colozza [6] compared power system options for a small lunar base camp and an ISRU oxygen production facility. Fincannon [7] characterized the lunar environment and corresponding lunar power needs for habitats, life support systems (LSS), laboratories, in-situ resource utilization (ISRU), and electrical vehicles. Therefore, effective energy resources are

* Corresponding author

required to supply the necessary electricity to the lunar community. Energy storage systems (ESSs) are also required to supply the loads in the evening and during eclipses. Designing a dependable and effective power system and integrating several energy resources and electrical equipment into a system complicated with multiple requirements are extremely difficult tasks, especially in light of the violent environment of space. Additionally, it might not always be feasible to have crew members with specialized knowledge in every field [8]. Therefore, a reliable power system achieves reliability, robustness, optimality, and stability. A space microgrid (MG) on the moon is an electrical power system composed of connected loads, energy-generating resources, and ESS [9]. Also, multi-MG (MMG) systems can be created by splitting various power-consuming equipment within a space MG among MMGs, each of which has its own local power generation and storage system. To improve the power system's flexibility and dependability, the MGs in an MMG system can combine their resources. Due to shortages of resources, only a few sources, including solar radiation and nuclear resources, can provide electricity on the Moon [6]. Static electricity from moon dust and fuel cells [10]. Nuclear kilo-power reactors are modular, light, and compact, and they don't depend on location or light. However, they need special shielding and must be placed far from the base to protect the crew from radiation [5]. Also, getting rid of nuclear waste is a problem, and we're still just testing how to get power from moon dust's static electricity [10]. The Moon's lack of atmosphere means plenty of solar energy reaches its surface. This solar radiation isn't impacted by things like clouds or atmospheric scattering. Plus, solar PV systems don't need heavy shielding, are easy to expand, and are already proven reliable in space. Although different spacecraft and rovers get their power from nuclear generators [11], the International Space Station, only human habitat in space, still gets its power from solar arrays and batteries [12]. The setup of solar power infrastructure for lunar bases is studied in [13]. For years, the world has been paying more attention to renewable energy because it's clean, widely available, and always there. Among these, solar (PV) energy is especially important and basic, mainly because sunlight is everywhere, plentiful, and sustainable [14]. With the increasing demand for solar energy on the grid and advancements in inverter technology, the emergence of larger solar power systems is anticipated. However, solar energy isn't constant, leading to power gaps, especially at night or in winter. This unsteady output makes grid stability and integration tricky. To boost reliability, an energy management plan using battery storage (BESS) and fuel cells can help keep power generation and demand in balance [15]. FC generation has become very popular in power systems because it is consistent in terms of cost and environmentally friendly. Solar arrays supported by regenerative fuel cells (RFCs) and batteries are highlighted in [16]. Even though solar systems with RFCs are lighter, RFCs are less efficient than batteries. Because batteries are more efficient, they charge faster during short sunlit periods. The design and sizing of power generation and storage for a human moon base are covered in [17]. In a recent study, an approach for determining the levelized cost of energy (LCOE) in a PV and BESS setup was presented [18]. This methodology is adapted in this research for space missions, with a fuel cell serving as the primary backup instead of a grid connection to ensure system reliability and dependability.

Contribution and Novelty

This study presents a comprehensive techno-economic analysis and optimal sizing of a PV–BESS–Fuel Cell hybrid system that is explicitly tailored to space microgrids on the lunar surface, rather than to generic Earth-based islanded systems. The proposed architecture includes a PV array, a battery energy storage system (BESS), an electrolyzer, a hydrogen storage tank, a hydrogen-based fuel cell, an inverter and a charge controller, coordinated by an energy management strategy that prioritizes direct PV supply, then battery charging, and finally hydrogen production and reconversion in the fuel cell during power deficits. The scientific contribution of the work goes beyond conventional PV–BESS–FC studies in several aspects:

- Space-specific resource and reliability constraints: The system is sized using illumination and temperature profiles representative of a lunar base, together with a

crewed-base load and a strict requirement of zero annual unserved energy. This captures multi-day eclipse periods, extreme temperature variations and the absence of atmospheric attenuation, which are not present in typical terrestrial microgrid analyses.

- Integrated LCOE–LCOS evaluation under lunar conditions: Levelized cost of energy (LCOE) and levelized cost of storage (LCOS) are calculated for PV, batteries and hydrogen storage under space operating conditions, identifying the most cost-effective combination of PV capacity and storage sizes for a lunar microgrid, rather than for Earth-based islands.
- Technology comparison with space-oriented performance criteria: Three battery technologies – lithium-ion, lead-acid and nickel-cadmium – are compared over a range of PV capacities using the same load, control strategy and reliability target. The analysis shows how the optimal technology choice changes when evaluated under lunar irradiance, temperature and long-duration autonomy requirements, instead of under terrestrial profiles.
- Inclusion of launch-mass and transportation-cost considerations: In contrast to Earth-based studies, where capital cost is usually the dominant economic factor, this work incorporates a mass-based model that links subsystem size (PV, BESS, hydrogen storage) to launch mass and transportation cost for delivery to the lunar surface. This explicitly demonstrates how heavier chemistries (lead-acid, Ni–Cd) become effectively non-competitive when mass penalties are accounted for, and why lithium-ion and hydrogen storage are preferred in a space context.

Taken together, these elements constitute the novelty of the work: the same PV–BESS–Fuel Cell architecture is analysed within a space-specific framework that combines lunar resource data, stringent reliability requirements and launch-mass-driven economics. This differentiates the study from Earth-based microgrid analyses and provides design insights that are directly relevant to future power systems for lunar surface missions. This work is considered a significant addition to previous research papers. While earlier works illustrated in **Table 1**.

Table 1. Summary of research papers on space power systems

Reference	Year	Description	Remarks / Limitations
[19]	2017	The paper establishes a common RFC architecture for different Mars and lunar surface locations. It highlights RFC's potential for Mars applications through ISRU integration and life support system interfaces and illustrates how its extended night time periods make it an essential component for lunar solar-based power systems.	The study presents preliminary trade results only and does not provide a full-sized design or performance model. It relies on state-of-the-art assumptions rather than simulated operation, and it does not quantify system-level economics, mass impacts, or long-duration lunar operational constraints.
[20]	2020	The paper provides a detailed analysis of EPSs for space microgrids, including sizing recommendations and the efficiency of solar cells with their types.	Focuses on satellite EPS architectures rather than surface habitats, and therefore does not model long-duration surface loads, hybrid storage, or planetary environmental constraints. No techno-economic assessment is performed, and regenerative or hydrogen-based storage is not evaluated.
[21]	2023	This research paper aims to minimize the Levelized Cost of	The system is grid-connected, terrestrial, and does not consider mass

		Energy (LCOE) while optimizing grid-connected PV-Battery Energy Storage Systems (BESS) using different types of battery.	constraints, extreme temperatures, radiation, or autonomy requirements. Results are not transferable to space microgrids, and long-duration energy storage beyond batteries is not addressed.
[1]	2023	This paper focuses on the optimal mass and size of PV arrays and batteries for a lunar microgrid at 15 highly illuminated sites near the lunar south pole, assuming 10 m high PV towers. It determines power demand profiles for In-Situ Resource Utilization (ISRU) for a 5-member crew.	Considers only PV and battery storage (no hydrogen subsystem), excludes operational degradation for some cases, and focuses primarily on mass optimization rather than full techno-economic evaluation. Does not integrate multi-storage architectures or compare battery technologies beyond capacity degradation.
This paper		Techno-economic analysis and optimal sizing of a hybrid lunar microgrid combining PV, BESS, electrolyzer, hydrogen storage, and fuel cell, with hourly simulation and evaluation of lithium-ion, lead–acid, and Ni–Cd batteries; includes mass-based launch assessment and LCOE/LCOS analysis.	This study develops an integrated techno-economic and mass-based sizing framework for lunar microgrids, uniquely combining PV generation, multi-chemistry battery assessment, and hydrogen long-duration storage. It links LCOE/LCOS with launch-mass impacts under hourly lunar conditions, offering design guidelines for reliable hybrid PV–BESS–hydrogen systems, but does not include long-term degradation, dust accumulation, or radiation effects.

CHOOSING A SITE FOR SPACE MGS ON THE MOON

A number of factors need to be carefully considered before establishing a human base on the moon. Partial and total eclipses, the length and frequency of lunar nights, and the radiation from the sun must all be taken into consideration. Important factors also include the site's location, the availability of water, and the capacity to successfully communicate with Earth. Temperature, day-night cycle, and sunlight intensity are the most important factors influencing PV cell energy generation in solar power. In addition, the severe conditions of space can seriously harm PV cells, resulting in early degradation and decreased performance. Therefore, the power production and degradation of the PV arrays must be considered when determining how much ESS is required to power things during eclipses.

Illumination

Assuming mass, volume, and mission cost are linked, a location with more light and shorter dark periods is preferred. This helps reduce the size of the ESS and overall mission expenses. Data from missions like NASA's Clementine, JAXA's Kaguya, and the Lunar Reconnaissance Orbiter (LRO) have been crucial in mapping the Moon's lighting. For instance, the Clementine mission found illuminated spots on the edge of the Peary crater at the Moon's North Pole [6]. Additionally, the Kaguya expedition located near the moon's south pole on the rim of the "Shackleton crater" that had the longest eclipse, lasting 11.5 Earth days, and 86% of the yearly average solar irradiation [9]. Similar to this, it has been shown that a few spots close to the Shackleton crater experience roughly six months of continuous sunshine and six months of

frequent swings between light and dark [16], with continuous eclipse times ranging from 71 to 120 hours [22]; it is better to be somewhere where the cycles of light and dark occur more frequently. Because ESSs may be quickly recharged during the light period, reducing the size of ESS that is required [22]. On the other hand, continuous light occurs on the lunar surface in non-polar regions for about 15 days, and then there is a continuous period of darkness for about 15 days [7]. Polar regions are therefore preferred for the construction of a lunar settlement since they require less ESS [23]. Additionally, by adding solar panels to towers, researchers have found a few areas where the ESS capacity can be decreased (see **Figure 1**) and finally eliminated entirely by raising the tower's height [24].

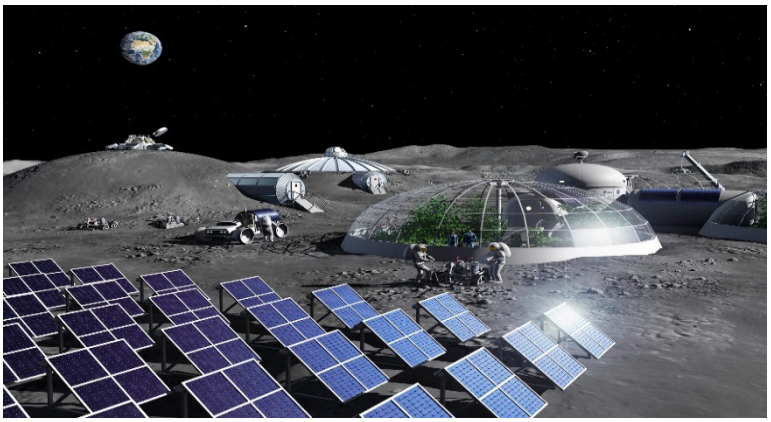

Figure 1. Mounting photovoltaic cells onto crater rim towers [25]

Theoretically, the ESS capacity can be lowered by 4% by constructing a 100-meter tower close to the lunar North Pole. Elevating the tower to a height of 300 meters can further lower the ESS operation period by 0.2 hours per meter. A 1500-meter tower close to the North Pole could do away with the need for an ESS. There is an alternative situation close to the South Pole that requires a 3000-meter tower to remove the requirement for ESS [22]. Building such tall structures will present a unique set of challenges, both in terms of mass and construction. While a well-lit site is preferred, the lunar base's construction should give it a position with the lowest meteoroid flow. Even if there is now a dearth of data from radars and spacecraft, the probability of meteorite impacts can still be estimated [26]. Compared to high latitudes, the chance of meteoroid fluxes is 10% higher at low latitudes. Thus, high light durations and fewer meteoroid impacts are characteristics of polar regions [27]. While it is impossible to completely prevent all catastrophic events, there are ways to make a design more robust, such as by using distributed, buried, and suitable shielding. These strategies are covered in [28]. A review of moon resource-based shielding techniques for lunar settlements with a mission of preventing meteoroid strikes is presented in [29].

Topography

Polar regions on the Moon are attractive for future spacecraft, but calculating how much solar power they can get is tough. This is because the sun stays just above the horizon near the poles. Consequently, it is imperative to understand the terrain surrounding a base, particularly within a 210 km radius. Even small hills nearby can cast kilometer-long shadows that might fully or partly cover the base. To help with this, we've mapped the Moon's surface using detailed digital elevation models (DEMs) from the LOLA experiment, as shown in **Figure 2**, [30]. It will be possible to calculate the solar energy availability at the base site with accuracy if the sun's route across the lunar polar horizon and the key relief's elevations are established. As a result, the best possible ESS sizing and energy management system may be put into place. Furthermore, the entire lunar nodal cycle, which lasts for around 18.6 years, should be considered because the ESSs must power all important loads even on a lunar day with the least amount of solar radiation.

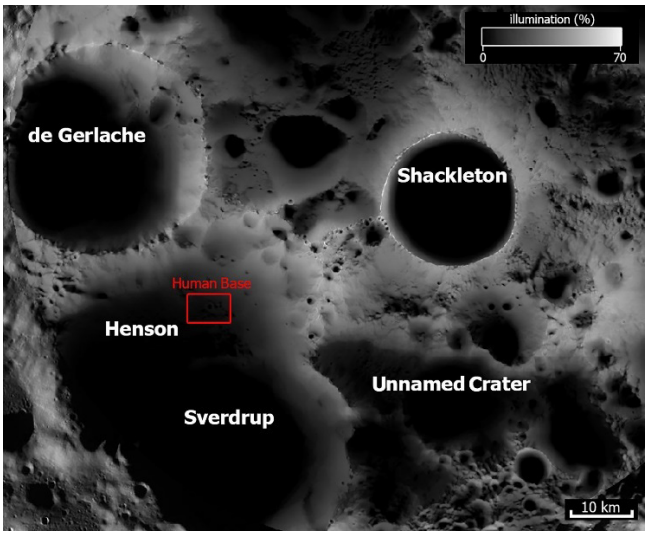

Figure 2. Topography of the moon [31]

Temperature

Accurate measurements of the base site temperature are critical for crew safety as well as for estimating energy output and consumption, which in turn maintains the stability of the spacecraft [32]. Accordingly, it has been suggested to use the regolith's physical characteristics and the profile of the sun's irradiation that reaches the lunar surface to calculate the temperature over the moon's surface [33], [34]. Another approximation relies on analytical models that consider the position of the sun and the empirically measured temperatures [35].

Power-Consuming Components of a Lunar Base

The lunar base is composed of different kinds of loads, or power-consuming devices. The crew habitat and base camp are associated with the most obvious loads. These include life support systems like heating, cooling, restoring the habitable atmosphere, and providing food and water to the astronauts, in addition to the power required for operating equipment like lights, computers, and experimental gear. Waste processing and biomass composting units are examples of additional LSS equipment that can significantly impact the total electrical consumption profile of the habitat [36]. Depending on the purpose, laboratories may also be part of the base [6]. In addition to specialist scientific instruments, the laboratories may contain other instruments resembling those in the habitat. Furthermore, electric vehicles that can accommodate humans can be employed for travel, maintenance, or site visits [7]. Electrical spacecraft that are autonomous or remotely controlled can also be employed to gather samples and conduct additional exploration of the lunar surface. Consequently, in order to charge these rovers and cars, charging facilities are required [7]. Systems for communication are among the other essential components of a lunar base. There should be a continuous connection between the base and the earthly ground station. Direct line of sight communication systems or orbiter spacecraft that gather data from the lunar base and transmit it to the earth's ground station are two ways that contact might be established. Various lunar establishments and units must also communicate with each other.

It is desirable to use locally available resources on the moon for extended lunar missions. Thus, it is possible to develop ISRU to extract oxygen and propellants from the regolith, which requires both heat and electrical power. Thermal power is needed to melt the lunar regolith within a boiler, but electrical power is needed to run the motors that collect, filter, and transport the regolith as well as the electrolysis. Electrical heaters can provide thermal power, but this option raises the need for electrical power. Alternatively, solar thermal systems may be employed, wherein solar radiation is directed and concentrated on a heat receiver that transfers the heat to a chamber for the melting of ilmenite [6]. In a different method, solar power is

focused onto optical waveguides composed of optical fibers using solar concentrators. The regolith receives solar radiation through the optical waveguide. Further details regarding the planning and execution of various solar concentrators for ISRU are available in [37], [39].

The lunar base habitat's power needs are contingent upon the number of crew members on board; for a crew of six, the projected requirement is 28.05 kW. A lunar base with less than ten crew members is anticipated to require a constant power source of about 35 kW. The ISRU requires 10 to 20 kW of electricity in order to create lunar propellants in the metric ton range. The power used by the ISRU can range from tens to hundreds of kW for both thermal and electrical power, depending on the production rate and process. According to estimates, the plant requires 9.3 kW of electrical power and 16.5 kW of thermal power to operate at a production rate of roughly 1.63 kg/h. In addition, a number of variables affect the amount of power needed by the rovers; it depends on factors such as their range, rate of discharge, ESS capacity, the terrain of the moon, and the physical properties of the regolith. The electric vehicle crew uses a system that may be pressurized for convenience, needing additional power resources. The transmission distance, data rate, bandwidth, and frequency of communication all affect how much power is needed for the communication systems. **Figure 3** and **Figure 4** list the maximum power of these systems for nonessential loads and also the power requirements for several consumption units demonstrated in **Table 2**.

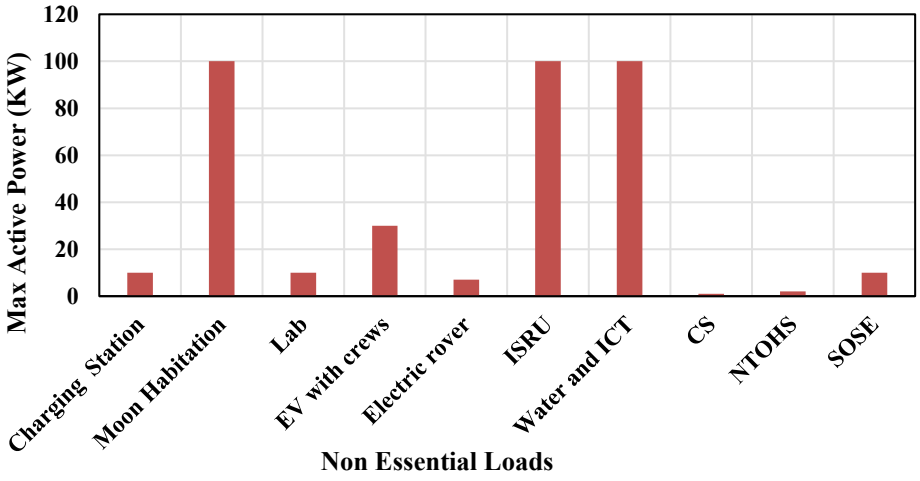

Figure 3. Maximum power for non-essential loads [5], [7]

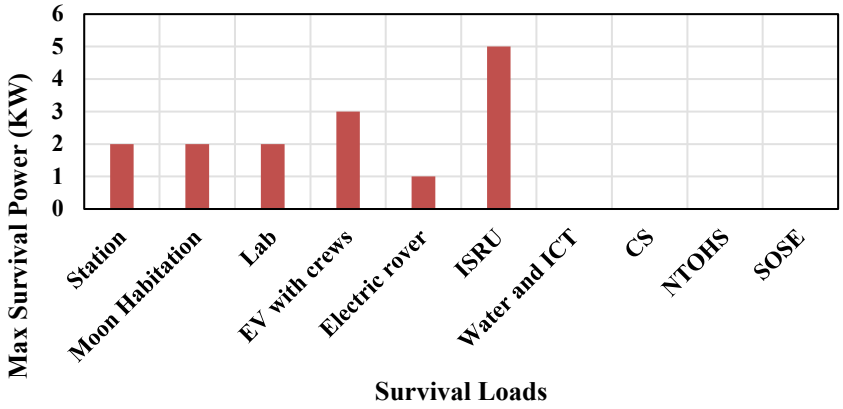

Figure 4. Maximum power for essential (Survival) loads [5], [7]

Table 2. Power Requirement to several consuming unit

Consuming unit	Representative power (from study)	Reference
Lunar habitat (4-crew First Lunar Outpost)	10 kW day, 9 kW night during crewed stay	[40]
Small lunar base camp (6-person, incl. labs & comms)	28.05 kW total base-camp power	[6]
ISRU oxygen production plant (1.63 kg/h O_2)	25.83 kW ISRU plant power	[6]
Human rover power system (small crewed rover)	1–3 kW (nominal 2 kW) rover power system	[41]
Water/ice exploration drill (Resource Prospector)	0.10–0.20 kW (100–200 W) for 1 m-class lunar drill	[42]
Initial exploration & science systems (incl. comms, robotics)	1–5 kW initial lunar power needs for exploration and lunar science	[43]

LEVELIZED COST OF ENERGY ECONOMIC METHOD

Figure 5 represents an FC unit with electrolysis, connected to a PV-BESS system comprising various components and supplying power to a load. The system also includes a hydrogen storage tank, an inverter, and a charging controller. The DC/AC inverter is required to transform a PV System's and FC DC outputs into AC so that electrical appliances can use it. The charge controller is vital for protecting the BESS against potential harm resulting from overcharging or under-discharging. In the current model, it assumes that the inverter efficiency remains constant, even though the fact that it could change. This study examines the hourly measurements of the solar radiation. An energy balance calculation is done for each hour of the year to determine how each hour's energy demand is provided just by the PV-BESS-FC. The electrical balances are calculated using a MATLAB R2014a simulation. The software runs scenarios for three different types of batteries: Lithium Ion Battery (Li-Ion), Lead-Acid Battery (LEAD), and Nickel-Cadmium (Ni-Cd).

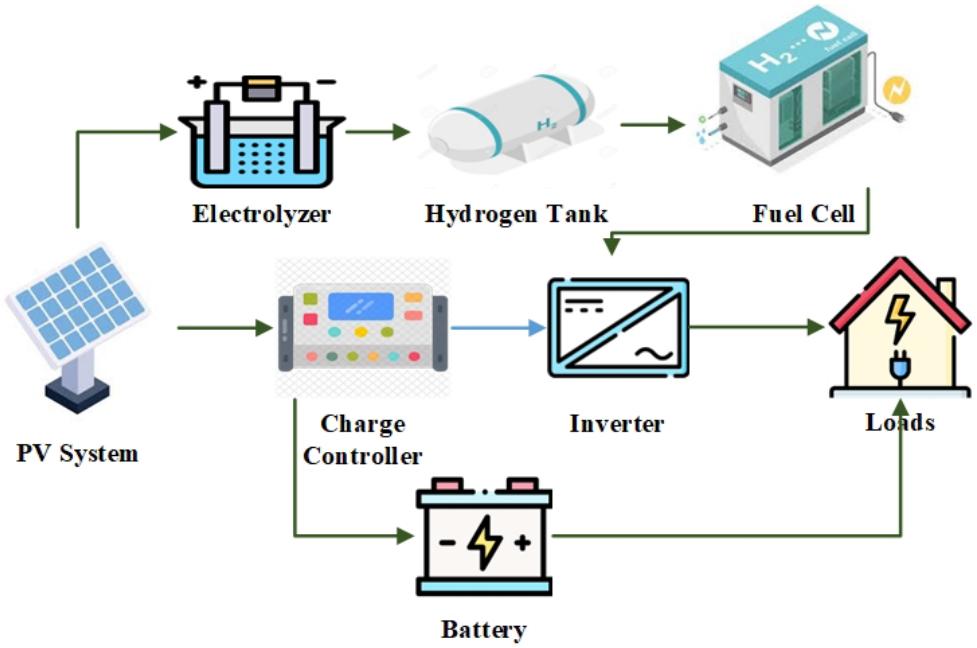

Figure 5. System configuration

A method involving iterative adjustments to the PV contribution is used to maximize the performance of the hybrid energy system shown in **Figure 5**. The solar power input is effectively varied using this technique. The simulation is specifically controlled across a range of PV system sizes by the variable P_{PVR}, which loops from 1 to 350 (P_{PVR}= 1:350). Using the formula $P_{PVr}= P_{PVr1} + 2 \times P_{PVR}$, where P_{PVr1} is an initial base power of 5 kW, the actual PV rated power (P_{PVr}) is determined for each step of P_{PVR}. Accordingly, the PV rated power begins at 7 kW (assuming P_{PVR}= 1) and rises by 2 kW every step, leading to at 705 kW (assuming P_{PVR} = 350). Additionally, the three different battery configurations Li-Ion, Lead-Acid, and Ni-Cd all go through this same procedure again. These distinct battery types are represented by the variable B_T in the code, which enables a comprehensive analysis of different storage technologies. The hybrid system's operational strategy is intended to effectively manage energy flow between its various components. The configuration that satisfies load requirements and delivers (LCOE) will be the most suitable. To satisfy the immediate load demand, the photovoltaic system first produces electricity. The main purpose of any extra PV power is to charge (BESS). The excess energy is then used by the electrolysis for producing hydrogen, which is then stored in the hydrogen tank, when the BESS reaches its maximum (SOC) or if there is still excess power. On the other hand, the BESS discharges to satisfy the power shortage when there is a PV deficit, which occurs when PV generation is not enough to meet the load. (FC) operates to produce electricity and guarantee a consistent supply to the load in the instance that the BESS reaches its minimum SOC or is unable to provide the necessary power. The FC draws hydrogen from the hydrogen tank. The proposed energy management system (**Figure 6**) operates on an hourly time step and follows a priority-based strategy that aims to maximise the direct use of PV power and minimise the use of stored energy. For each simulated hour, the algorithm first reads the irradiance, temperature and load data, configures the PV system and initialises the result arrays. For every combination of PV size and battery type, the loop then evaluates the available PV power P_{PV} and the instantaneous load demand P_L. If $P_{PV}>P_L$, the excess power is calculated. The controller first checks whether the battery is not fully charged; if so, it charges the BESS up to its maximum allowable state of charge. If further surplus power remains and the hydrogen tank is not full, this excess is sent to the electrolyser to produce hydrogen and charge the tank. Only when both storage elements are at their upper limits is the PV operating point adjusted (curtailment) to avoid overproduction. Conversely, if $P_{PV} < P_L$, a power deficit is computed. The controller then checks whether the battery has sufficient stored energy; when this is the case, the BESS is discharged to reduce or eliminate the deficit. If the battery cannot fully cover the deficit, the controller verifies whether the hydrogen tank contains enough energy; if so, the fuel cell is started and the required power is generated from stored hydrogen. Only when neither the BESS nor the hydrogen tank can provide sufficient power is load shedding applied as a last resort. At the end of each hour, all energy flows (production, charging/discharging, electrolysis, fuel-cell output, curtailment and unserved load) are stored for plotting and for the subsequent techno-economic analysis.

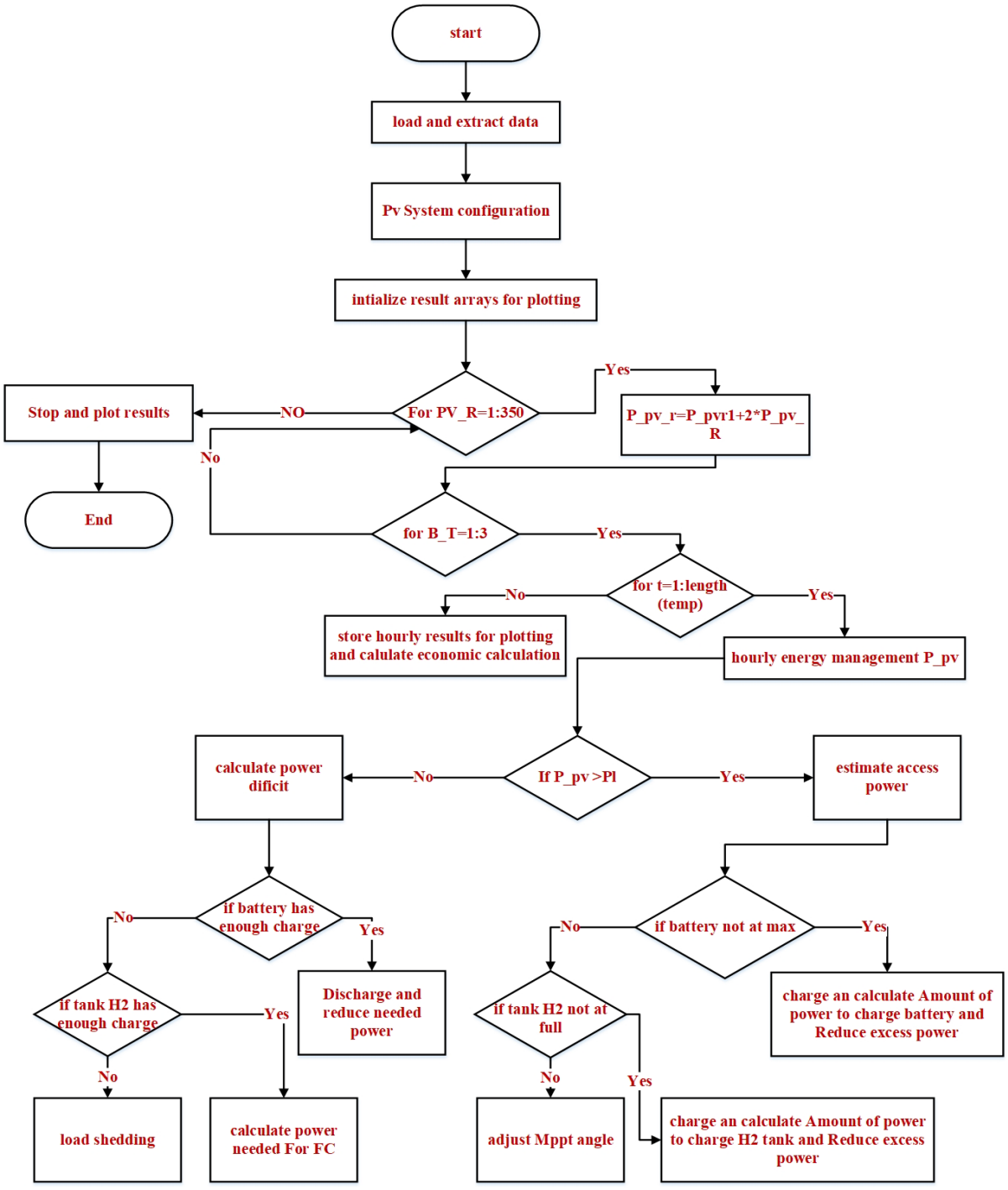

Figure 6. Proposed energy management system for the hybrid energy system

SYSTEM MODEL

This section presents an integrated power architecture system model of an autonomous lunar power generation system consisting of each of the following subsystems: photovoltaic (PV) generation, battery energy storage (BESS), and proton-exchange membrane fuel cell (PEMFC) with electrolytic hydrogen generation/storage. It translates the component-level physics, efficiencies and temperature effects; operating states and state-of-charge (*SOC*) limits for both batteries and the hydrogen tank; and the power-flow logic which controls charging, discharging and eclipse operation. Finally, a levelized cost of energy (LCOE) methodology is developed that accumulates lifetime capital costs, replacement costs and O&M costs across all subsystems for assessment of competing design alternatives on a consistent economic basis.

Photovoltaic Model

The hourly power generated by the PV arrays is a function of PV system efficiency (detailed in [44]), solar irradiation at the PV installation location, and the solar power system area (in m²). According to [44], η_{pv} is determined by a few constant variables, such as module efficiency (η_{m}), including project lifetime (LT), inverter efficiency (η_{inv}), and the degradation of the PV system (Deg_{pv}), and temperature efficiency (η_{temp}), is a time variable. Multi-Junction Gallium Indium Phosphide/Gallium Arsenide/Germanium Solar Cell (MJGaInP/GaAs/Ge) solar panels are widely used in space applications [45].

$$P_{\mathrm{pv,t}} = I_{\mathrm{pv,t}} \times A \times \eta_{\mathrm{pv,t}} \tag{1}$$

$$\eta_{\mathrm{pv,t}} = \eta_{\mathrm{m}} \times \eta_{\mathrm{temp}} \times (1 - (LT - 1) \times Deg_{\mathrm{pv}} \tag{2}$$

$$\eta_{\mathrm{temp,t}} = [1 - \beta \times (T_{\mathrm{cell,t}} - T_{\mathrm{ref}})] \tag{3}$$

$$T_{\mathrm{cell,t}} = T_{\mathrm{amb,t}} + \frac{[(NOT - T_{\mathrm{amb,NOT}})]}{[I_{\mathrm{NOT}}]} \times I_{\mathrm{pv,t}} \tag{4}$$

$$A = \frac{P_{\mathrm{pv,r}}}{\eta_{\mathrm{m}} \times SR} \tag{5}$$

where, $P_{\mathrm{pv,r}}$ is the rated PV output power (kW), and SR donates to constant solar radiation, which is often considered to be 1.359 kW/ m² [6], the β term to represent the photovoltaic cell efficiency temperatures coefficient (1/℃), while [34] uses NOT to represent the typical operating temperature of a cell (℃), T_{ref} represent the reference temperature for photovoltaic cells (℃), and uses T_{cell} to represent the temperature of the solar cell.

Battery Energy Storage System Model

There are various types of ESSs that can be used in space applications. The typical daily demand informs the battery capacity based on the desired hours of autonomy (HA), which represents the duration a fully charged battery can continuously power the load:

$$B_{\mathrm{cap}} = \frac{HA \times P_{\mathrm{l,avg}}}{\eta_{\mathrm{inv}} \times \eta_{\mathrm{dch}} \times DOD} \tag{6}$$

where $P_{\mathrm{l,avg}}$ is the average load demand (kW) and is calculated by dividing the annual demand by the yearly number of hours. DOD represents the depth of discharge, set at 80% for all three batteries (Li-Ion-LEAD and NI-Cd), and η_{inv} and η_{dch} are the inverter efficiency and battery discharge efficiency, respectively. SOC is utilized to determine whether to charge or discharge the battery. To determine the battery's SOC, a continuous energy balance is necessary. The load is primarily supplied by PV power. If the PV system generates more energy than the load requires ($P_{\mathrm{pv}} > P_{\mathrm{l}}$), the excess power is used to charge the battery. The SOC during charging can be expressed as follows:

$$SOC_t = SOC_{t-1} + (P_{\mathrm{pv},t} - P_{\mathrm{l},t}) \times \eta_{\mathrm{ch}} \times \eta_{\mathrm{inv}} \tag{7}$$

where are the BESS respective states of charge at times t and time t-1. Compared to that, if ($P_{\mathrm{pv}} < P_{\mathrm{l}}$), the energy generated by PV will be used to meet the load, and any shortage will be made up from the BESS. The battery SOC during discharging mode is shown:

$$SOC_t = SOC_{t-1} - \frac{P_{\mathrm{pv},t} \times P_{\mathrm{l},t}}{\eta_{\mathrm{inv}} \times \eta_{\mathrm{dch}}} \quad (8)$$

The following constraints apply to the battery SOC at any time t:

$$SOC_{\min} < SOC_t < SOC_{\max} \quad (9)$$

Here, $SOC_{\min}$ and $SOC_{\max}$ define the permissible range for the state of charge, representing the minimum and maximum values. For the simulation, the initial *SOC* for each of the three batteries is set to $SOC_{\text{ initial}}$.

Fuel Cell with Hydrogen Tank and Electrolysis Model

Due to their suitability for space applications, this work focus on proton-exchange membrane fuel cells (PEMFCs) in the current study, which is adapted from [6] for five crew members. Similar to a flow battery, a fuel cell (FC) stack converts chemical energy into direct current electricity. This process is reversed by electrolysis, which converts electrical power back into chemical energy. Nevertheless, in addition to the wanted energy conversion, both of these processes generate heat and chemical byproducts, making them neither completely efficient. (PV) array output is the initial source of power for the current system. If necessary, the battery is charged using any excess power. If necessary, the hydrogen tank can be charged using the battery or the PV array. When there is an eclipse, at night, or when there is a deficit, the system uses the battery or PV to generate power. When the hydrogen tank is empty, the PEMFC converts the hydrogen back into energy for the load. Equations below describe how this process also generates heat for drinking water and heating:

$$2H_2O + \text{Electricity} \Rightarrow 2H_2 + O_2 \quad (10)$$

$$\eta_{\text{Electro}} = \frac{\text{Chemical Energy}}{\text{PV Output power}} 2H_2O + \text{Heat} \quad (11)$$

$$\eta_{\text{Electro}} = \frac{\text{Chemical Energy}}{\text{PV Output power}} \quad (12)$$

$$\eta_{\text{FC}} = \frac{\text{Electrical power}}{\text{Chemical Energy}} \quad (13)$$

The capacity of the hydrogen tank is defined in kilograms and then converted to kilowatt-hours based on the energy content of hydrogen:

$$E^{\text{kwh}}_{\text{H}_2,\text{tank}} = M^{\text{kg}}_{\text{H}_2,\text{tank}} \times 33.3\ k\text{wh/kg} \quad (14)$$

where $E^{\text{kwh}}_{\text{H}_2,\text{tank}}$ is the hydrogen tank capacity in kwh, $M^{\text{kg}}_{\text{H}_2,\text{tank}}$ is the hydrogen tank capacity in kg and 33.3 kWh/kg represents the Lower Heating Value (LHV) of hydrogen. The *SOC* for the hydrogen tank is crucial for managing the hydrogen supply to the fuel cell and its replenishment by the electrolysis. The *SOC* during charging via the electrolysis (when surplus PV power is available) can be expressed as follows:

$$SOC_{\text{H}_2}(t) = SOC_{\text{H}_2}(t-1) + P_{\text{Electrolysis}}(t) \times \eta_{\text{electrolysis}} \quad (15)$$

where $SOC_{\mathrm{H}_2}(t)$ and $SOC_{\mathrm{H}_2}(t-1)$ are the hydrogen tank respective states of charge at times *t* and *t*−1. $P_{\mathrm{Electrolysis}}(t)$ is the power consumed by the electrolyzer at time *t*, $\eta_{\mathrm{electrolysis}}$ is the electrical efficiency of the electrolysis, compared to that, if the system requires power not met by PV or battery (i.e., a power deficit requiring fuel cell operation), the energy deficit will be made up from the hydrogen tank via the fuel cell. The hydrogen tank *SOC* during discharging mode (fuel cell consumption) is shown:

$$SOC_{\mathrm{H}_2}(t) = SOC_{\mathrm{H}_2}(t-1) - \frac{P_{\mathrm{FC}(t)}}{\eta_{\mathrm{FC}}} \tag{16}$$

where $P_{\mathrm{FC}(t)}$ is the power output from the fuel cell at time *t*, and η_{FC} is the electrical efficiency of the fuel cell. The following constraints apply to the hydrogen tank *SOC* at any time *t*;

$$SOC_{\mathrm{H}_{2,\min}} < SOC_{\mathrm{H}_2}(t) < SOC_{\mathrm{H}_{2,\max}} \tag{17}$$

where $SOC_{\mathrm{H}_{2,\min}}$ and $SOC_{\mathrm{H}_{2,\max}}$ define the permissible range for the *SOC*, representing the minimum and maximum values, all these equations under main constraints considering P_{C} and P_{d} charging and discharging power of battery:

$$P_{FC} + P_{pv} + P_d = P_{consumption} + P_C \tag{18}$$

Levelized Cost of Energy Economic Model (LCOE)

The LCOE is a standard method for evaluating the financial feasibility of PV-BESSs, FC with electrolysis and hydrogen tank. It provides a more accurate economic assessment by spreading project costs across the entire operational life [46], [48]. In a stand-alone PV-BESS-FC system, the LCOE can be calculated by dividing all system costs by the amount of energy produced [48]. In the current study, PV energy generated is dynamically utilized to, directly supply the electrical load, recharge the (BESS), power the electrolysis for hydrogen production and storage in the hydrogen tank in terms of $E_{\mathrm{pv,l}}$, total lifetime discounted electrical energy from PV directly supplied to the load, $E_{\mathrm{pv,Ch}}$, total lifetime discounted electrical energy from PV going to charging (batteries or electrolysis), E_{BESS}, total life time discounted electrical energy discharged from the BESS, E_{FC}, total lifetime discounted electrical energy produced by the Fuel Cell over its lifetime, and $E_{\mathrm{Electrolysis}}$ total lifetime discounted electrical energy input to the electrolysis. The total system cost consist of the sum of discounted capital costs, operation & maintenance (O&M) costs, fuel costs, and replacement costs for all components, this include (C_{BESS}) total lifetime cost of the (BESS), includes initial installation cost and discounted annual O&M costs, ($C_{\mathrm{pv,T}}$) total lifetime cost of the PV modules and inverter, plus annual PV O&M, (C_{FC}), total lifetime cost of the Fuel Cell (FC) system, plus annual FC O&M, ($C_{\mathrm{Elecctroysis}}$), total lifetime cost of the Electrolysis system, plus annual electrolysis O&M and replacement costs, ($C_{\mathrm{H_2tank}}$), total lifetime cost of the Hydrogen Storage Tank, plus annual H_2 tank O&M, the suggested design adapts the LCOE solution for application in a FC-connected PV-BESS. Relations below are used to derive the proposed system LCOE and determine the most economical system, a step by step for system LCOE is given as follows:

$$C_{\mathrm{pv,T}} = [\, C_{\mathrm{pv,inst}} + \sum_{J=0}^{J=\mathrm{LT}} \frac{C_{\mathrm{PV,O\&M}}}{(1+r)^J} \,] \tag{19}$$

$$E_{\mathrm{pv,l}}=\sum_{J=0}^{J=\mathrm{LT}}\frac{E_{\mathrm{PV,L},J}(1-DEG_{\mathrm{PV}})^{J}}{(1+r)^{J}} \tag{20}$$

$$E_{\mathrm{pv,Ch}}=\sum_{J=0}^{J=\mathrm{LT}}\frac{E_{\mathrm{PV,Ch},J}(1-DEG_{\mathrm{PV}})^{J}}{(1+r)^{J}} \tag{21}$$

$$C_{\mathrm{BESS}}=[\,C_{\mathrm{B,inst}}+\sum_{J=0}^{J=\mathrm{LT}}\frac{C_{\mathrm{B,O\&M}}}{(1+r)^{J}}\,] \tag{22}$$

$$E_{\mathrm{BESS}}=\eta_{\mathrm{rt}}\sum_{J=0}^{J=\mathrm{LT}}\frac{E_{\mathrm{PV,Ch},J}(1-DEG_{\mathrm{B}})^{J}}{(1+r)^{J}} \tag{23}$$

$$C_{\mathrm{FC}}=[\,C_{\mathrm{FC,inst}}+\sum_{J=0}^{J=\mathrm{LT}}\frac{C_{\mathrm{FC,O\&M}}}{(1+r)^{J}}\,] \tag{24}$$

$$E_{\mathrm{FC}}=\sum_{J=0}^{J=\mathrm{LT}}\frac{E_{\mathrm{FC},J}(1-DEG_{\mathrm{FC}})^{J}}{(1+r)^{J}} \tag{25}$$

$$C_{\mathrm{Elecctroysis}}=C_{\mathrm{Elecctroysis,inst}}+\sum_{J=0}^{J=\mathrm{LT}}\frac{C_{\mathrm{Elecctroysis,O\&M}}}{(1+r)^{J}} \tag{26}$$

$$E_{\mathrm{Electrolysis}}=\sum_{J=0}^{J=\mathrm{LT}}\frac{E_{\mathrm{Electrolysis},J}}{(1+r)^{J}} \tag{27}$$

$$C_{\mathrm{H_2tank}}=C_{\mathrm{H_2tank,inst}}+\sum_{J=0}^{J=\mathrm{LT}}\frac{C_{\mathrm{H_2tank,O\&M}}}{(1+r)^{J}}\,] \tag{28}$$

$$\mathrm{LCOE}_{\mathrm{E_{PV}}}=\sum_{J=0}^{J=\mathrm{LT}}\frac{C_{\mathrm{pv,T}_J}}{E_{\mathrm{pv,l}}+E_{\mathrm{pv,Ch}_J}} \tag{29}$$

$$\mathrm{LCOS}=\sum_{J=0}^{J=\mathrm{LT}}\frac{C_{\mathrm{BESS}_J}}{E_{\mathrm{BESS}_J}} \tag{30}$$

$$\mathrm{LCOE}_{\mathrm{FC}}=\sum_{J=0}^{J=\mathrm{LT}}\frac{C_{\mathrm{FC}_J}}{E_{\mathrm{FC}_J}} \tag{31}$$

$$\mathrm{LCOE}_{\mathrm{SYS}}=\frac{C_{\mathrm{pv,T}}+C_{\mathrm{BESS}}+C_{\mathrm{FC}}+C_{\mathrm{Elecctroysis}}+C_{\mathrm{H_2tank}}}{\mathrm{Total\_Load\_Served}} \tag{32}$$

Mass and Transportation Cost Estimation

For lunar surface missions, launch mass is a primary driver of feasibility and overall cost. Jones [49] shows that, for a Moon base architecture using Falcon Heavy, the effective cost to deliver payload to the lunar surface is approximately 10.8 kUSD/kg, obtained by combining a low-Earth-orbit launch cost of 1.52 kUSD/kg with a mass ratio of 7.2 from LEO to the lunar

surface. This subsection introduces a simplified mass and transportation-cost model for the main subsystems of the proposed PV−BESS− H_2 − FC microgrid.

Battery mass. Let C_B denote the nominal battery energy capacity at pack level (kWh) and e_{spec} the pack-level specific energy (Wh/kg). The corresponding battery mass M_{BESS} is approximated by:

$$M_{\mathrm{BESS}} = \frac{C_{\mathrm{B}}[\mathrm{kWh}] \times 1000}{e_{\mathrm{spec}}[\ \mathrm{Wh/kg}]} \tag{33}$$

This follows directly from the definition of specific energy.Typical reported pack-level specific energy ranges are:

- Lithium-Ion (Li-Ion): $= 150 - 250$ Wh/kg at cell/pack level in state-of-the-art EV cells [50], [51].
- Lead-Acid: $= 30 - 50$ Wh/kg for traction and stationary applications [52], [53].
- Nickel-Cadmium (Ni-Cd): $= 40 - 60$ Wh/kg for conventional industrial Ni-Cd cells [53], [54].

In the results, mid-range values within these intervals are adopted to obtain indicative battery masses for Li − Ion, Lead-Acid, and Ni − Cd chemistries at the same nominal capacity C_B.

PV array mass. For space PV technology, subsystem mass is commonly related to peak electrical power via the specific power σ_{PV}(W/kg). Lightweight arrays based on III-V multijunction cells and flexible blanket structures have demonstrated specific powers on the order of $100 - 150$ W/kg and power densities around $300 - 350\mathrm{W/m^2}$. For example, Law *et al.* [55] report specific power values around 150 W/kg for thin, flexible III-V multijunction panels, and Mikulas *et al.* [56] adopt similar figures in the context of high-specific power telescoping solar arrays for deep-space missions [57].

For a PV array rated at P_{PV}(kW), the PV array mass is estimated as:

$$M_{\mathrm{PV}} = \frac{P_{\mathrm{PV}}[\ \mathrm{kW}] \times 1000}{\sigma_{\mathrm{PV}}[\ \mathrm{W/kg}]} \tag{34}$$

In the subsequent calculations, a specific power $\sigma_{PV} = 150\ \mathrm{W.kg^{-1}}$ is used, representative of highperformance flexible blanket arrays reported in [55], [57].

Hydrogen energy content and storage mass. Hydrogen is characterised by a lower heating value (LHV) of approximately $120\mathrm{MJ \cdot kg^{-1}}$, corresponding to about 33.3 kWh/kg. For a stored hydrogen mass m_{H2}(kg), the chemical energy content E_{H2} is therefore [58]:

$$E_{\mathrm{H2}} = m_{\mathrm{H2}} \times 33.3\ \mathrm{kWh/kg} \tag{35}$$

High-pressure compressed hydrogen storage for mobile applications is typically implemented using Type-IV composite tank systems. Hua *et al.* [59] analyse a 700 bar onboard storage system that stores 5.6 $\mathrm{kgH_2}$ with a system gravimetric capacity of 4.2 wt% and a system-level specific energy of 1.40 kWh/kg. This corresponds to a total system mass of approximately $M_{sys,ref} = 133.6$ kg, for 5.6 kg of stored hydrogen [59]. Assuming linear scaling of tank-system mass with stored hydrogen mass (a standard first-order approximation for conceptual design), the mass of a tank system capable of storing m_{H2} is estimated as:

$$M_{\mathrm{H2,sys}} = m_{\mathrm{H2}} \times \frac{133.6\ \mathrm{kg}}{5.6\ \mathrm{kgH_2}} \tag{36}$$

The corresponding system-level specific energy for the hydrogen storage subsystem is then:

$$e_{\mathrm{H2,sys}} = \frac{E_{\mathrm{H2}} \times 1000}{M_{\mathrm{H2,sys}}} \ [\ \mathrm{Wh/kg}] \tag{37}$$

which can be directly compared with the pack-level specific energies e_{spec} of the electrochemical BESS technologies.

Total system mass and transportation cost. The total launch mass of the power system is written as the sum of the main subsystems:

$$M_{\mathrm{tot}} = M_{\mathrm{PV}} + M_{\mathrm{BESS}} + M_{\mathrm{FC}} + M_{\mathrm{ELZ}} + M_{\mathrm{H2,sys}} + M_{\mathrm{BoP}} \tag{38}$$

where $M_{\mathrm{FC}}, M_{\mathrm{ELZ}}$ and M_{BoP} represent the masses of the fuel-cell stack, electrolyzer, and balance-of-plant (mounting structures, cabling, power-conditioning equipment, etc.), respectively. For the comparison between battery chemistries, these latter terms can be considered approximately common, since they depend mainly on rated power and hydrogen throughput rather than on the specific choice of battery technology.

For a given cost per kilogram to the lunar surface $c_\ell(\mathrm{USD/kg})$, the transportation cost contribution of subsystem i is defined as:

$$C_{\ell,\mathrm{i}} = c_\ell M_{\mathrm{i}} \tag{39}$$

Using the value $c_\ell = 10.8$ kUSD/kg reported by Jones [49] for a Moon base architecture, the mass differences between alternative battery and storage technologies can be directly translated into launch-cost differences.

RESULTS AND DISCUSSION

This section presents the results of the simulation and interprets the implications of the results for the case of a standalone PV-BESS-PEMFC system with electrolytic hydrogen storage. Using solar irradiance and temperature profiles representative of space, three storage options were compared (Li-Ion, Lead-Acid, and Ni-Cd) for multiple ratings of PV systems, report subsystem energy flows, and quantify costs with LCOE/LCOS. The configurations that minimize lifecycle energy costs and unserved load analyze the operational behavior of the fuel cell, electrolyzer, and hydrogen tank state of charge (SOC).

This method aims to optimize the sizing and evaluate the economic feasibility of a hybrid energy system PV-BESS and fuel cell systems with hydrogen tank. This study considering three types of batteries: Li-Ion, LEAD, and Ni-Cd. These simulations employ solar radiation data in **Figure 7** and a simplified effective ambient temperature profile (**Figure 8**) representing the thermally controlled environment of the equipment bay (power-conditioning units, BESS enclosure, fuel cell and electrolyser balance of plant), rather than raw lunar surface or crew cabin temperatures. In this context, the peak value of 40 °C shown in **Figure 8** corresponds to a worst-case equipment-enclosure temperature within the allowable operating range of space-qualified electronics and batteries, while the habitable volume itself is assumed to be maintained near human comfort conditions (20 – 23 °C) by the habitat thermal control system. The suggested framework is implemented through multiple simulations in MATLAB 2014a, specifically regarding the three scenarios: PV- Li-Ion, PV-LEAD, and PV-Ni-Cd. All batteries are rechargeable batteries commonly used for storage in space applications. The electrical demand is represented by an annual hourly load

profile for the lunar base (**Figure 9**), comprising 8,760 hourly point. The study assumes a system lifetime of 20 years, with the batteries, inverter, and charge controller being replaced at 10 and 20 years. The battery capacities are calculated using eq. **(6)** for a 5-hour autonomy period. **Table 3** displays all PV system parameter values, while **Table 4** displays the LI-Ion, LEAD, and NI-Cd specifications assumed that all batteries possess a capacity of 2.5 MWh, plus **Table 5** displays FC with Electrolysis and hydrogen tank CHARACTERISTICS. After conducting the simulations. it becomes clear that the proposed technical and economic model, especially with the combining of ESSs such as BESS and FC with electrolysis, demonstrates promising results in achieving sustainability and economically meeting the load demand, and this illustrated in **Table 6**.

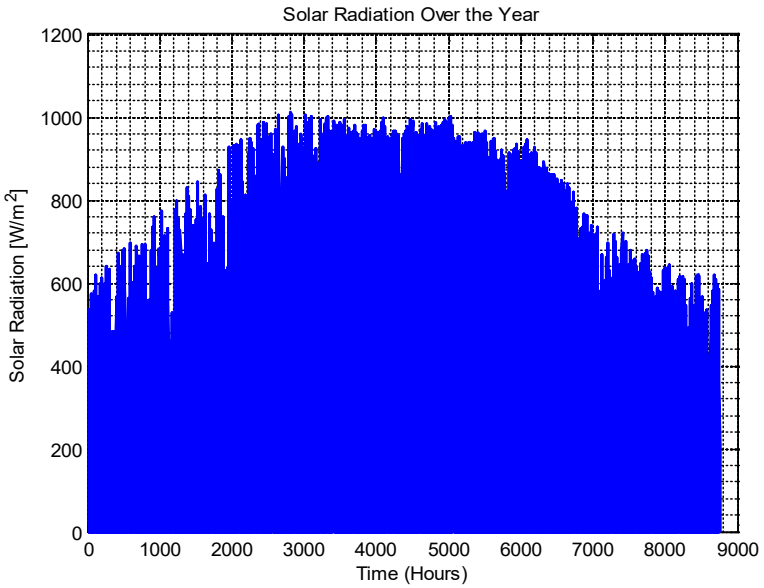

Figure 7. Solar radiation of space nature

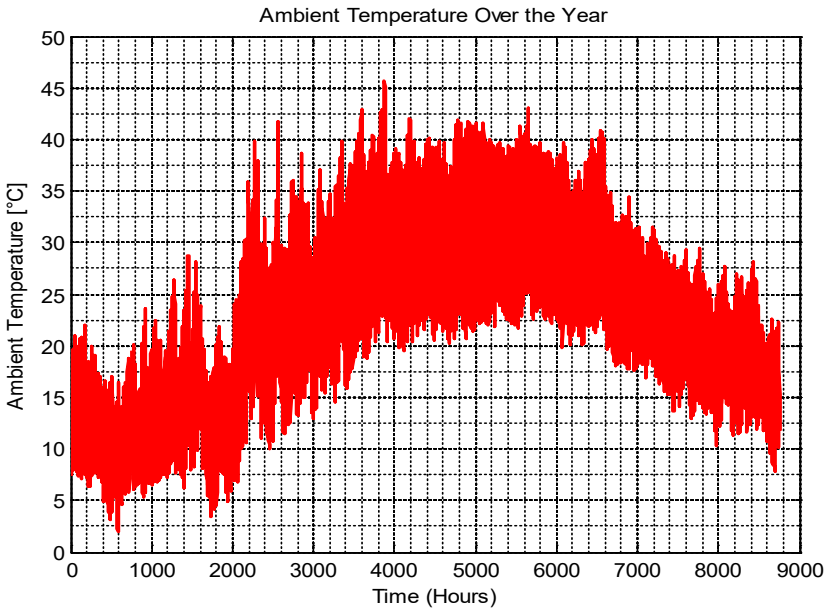

Figure 8. Hourly ambient temperature profile

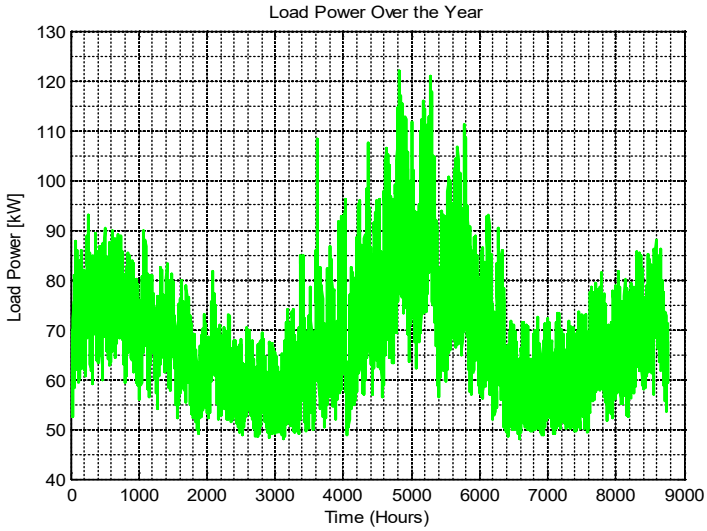

Figure 9. Load demand profile

Table 3. Solar system characteristics' specifics [1], [60], [62]

Parameter	Value/Range	Parameters	Value/Range
$\boldsymbol{P_{PV,rated}}$	5 - 700 kW, step 2 kW	C_{pv}	$P_{PV} \times 2828 \times P_{PV}^{-0.128}$
$\boldsymbol{\eta_{pv}}$	28%	C_{inv}	$1.1P_{PV} \times Pr_{inv}$
$\boldsymbol{\eta_{inv}}$	92%	pr_{inv}(Inverter Price)	0.56 USD/W
$\boldsymbol{DEG_{PV}}$(PV degradation rate)	0.3%	$C_{pv,inst}$	$C_{pv} + C_{inv}$
$\boldsymbol{B}$ (Temperature coefficient for PV)	0.005/℃	$C_{pv,O\&M}$	1% of $C_{pv,inst}$
$\boldsymbol{P_{rcc}}$(Charge controller price per Ampere)	4.62 USD/kWh	$C_{inv,rep}$(Inverter Replacement Cost)	C_{inv} for J=10&20
$\boldsymbol{C_{cc}}$(Charge controller cost)	$(P_{PV}/V_b) \times P_{rcc}$	T_{ref}	25 ℃
NOCT	45 ℃	*LT* (life time)	20 Years
$\boldsymbol{P_{L,avg}}$	69.72 kW	*HA*	5 Hours
H	1359 WH/M^2	*r* (Discount rate)	6%

Table 4. Batteries characteristics [1], [48]

Parameter	Lithium-Ion (Li-Ion)	Lead-Acid (LEAD)	Nickel-Cadmium (Ni-Cd)
$\boldsymbol{\eta_{rt}}$	90%	80%	85%
$\boldsymbol{DEG_B}$	0.5%	1.6 %	0.8%
Lifetime	5-20	5-15	10-15
$\boldsymbol{C_{B,inst}}$	600 USD/ kWh	100 USD/ kWh	1000 USD/ kWh
$\boldsymbol{C_{B,O\&M}}$	1%	5%	2%
CB		2.5 MWh	

Parameter	Lithium-Ion (Li-Ion)	Lead-Acid (LEAD)	Nickel-Cadmium (Ni-Cd)
$\boldsymbol{CB_{rep}}$		$C_{B,inst}$ for J=10&20	
$\boldsymbol{SOC_{min}}$		20%	
$\boldsymbol{SOC_{max}}$		100%	
DOD		80%	

Table 5. FC with Electrolysis and hydrogen tank characteristics [6], [63], [66]

Parameter	Value/Range
$\boldsymbol{\eta_{Electrolysis}}$	85%
$\boldsymbol{\eta_{FC}}$	65%
$\boldsymbol{C_{FC,inst}}$	1200 USD/kW
$\boldsymbol{C_{Fc,O\&M}}$	2%
Lifetime	10
$\boldsymbol{DEG_{FC}}$	8%
$\boldsymbol{C_{Electrolysis,inst}}$	1500 USD/kW
$\boldsymbol{C_{Electrolysis,O\&M}}$	1%
H_2 tank capacity in kg	18.6
H_2 energy kWh per kg	33.3
Initial State of Charge for H_2 tank	20%
Capital cost per kg for hydrogen storage	50 USD/kg
O&M cost fraction for H_2 tank	0.5%

Table 6. Results in achieving sustainability and economically meeting the load demand

Energy produced from PV to Load	301.45 MWh
System LCOE (Levelized Cost of Energy)	0.2379 USD/kWh
Total Electrical Load Served	610.73 MWh
Energy produced from Fuel Cell (FC)	93.42 MWh
Total Energy produced from PV	801.22 MWh
Total Battery Energy Discharged	176.07 MWh
Total Battery Energy Charged	191.38 MWh
Hydrogen Tank Energy Charged (from Electrolysis input)	306.41 MWh
Hydrogen Tank Energy Discharged (to Fuel Cell)	143.72 MWh

Figure 10 shows the system LCOE for several battery types over a variety of PV rated powers. The Li-Ion battery always displays the lowest LCOE, at a minimum of 0.13181 USD/kWh for 7.0 kW PV power. Li-Ion is the most cost-effective option for this system, as shown by the fact that it is superior to Ni-Cd (min. 0.16561 USD/kWh) and lead-acid (min. 0.23449 USD/kWh).

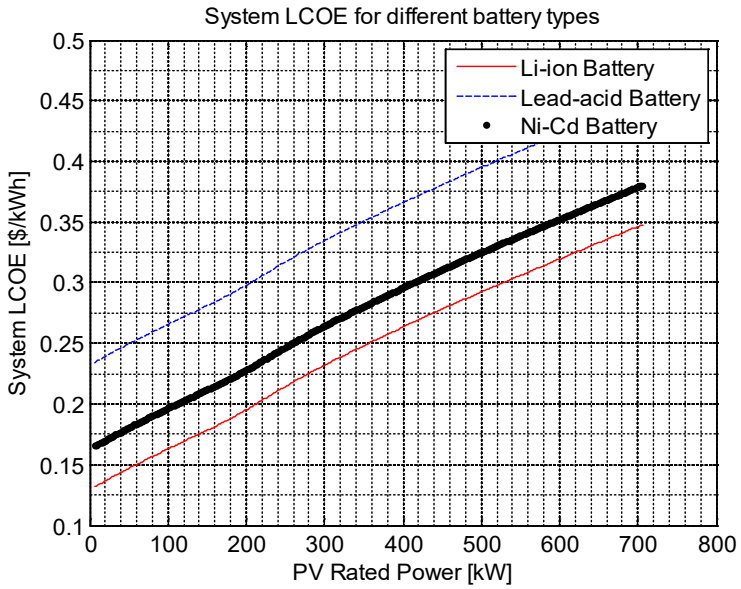

Figure 10. Levelized cost of energy of the FC- PV-BESS

According to **Table 7**, PV-Li-ion batteries have the lowest overall system LCOE (USD 0.2379), followed by PV-Ni-Cd (USD 0.2717) and PV-Lead-Acid (USD 0.3406). This demonstrates that Li-Ion is the least costly option. The LCOE specifically from the PV component (PV LCOE) is shown in the **Figure 11**. All battery types have the same cost, which drops as the rated power of the PV system rises to 0.0815 USD/kWh at higher capacities. This indicates that the size of the solar cells alone determines how much it costs to produce electricity, also **Table 8** presents LCOS in USD/kWh for the 3 different types of batteries.

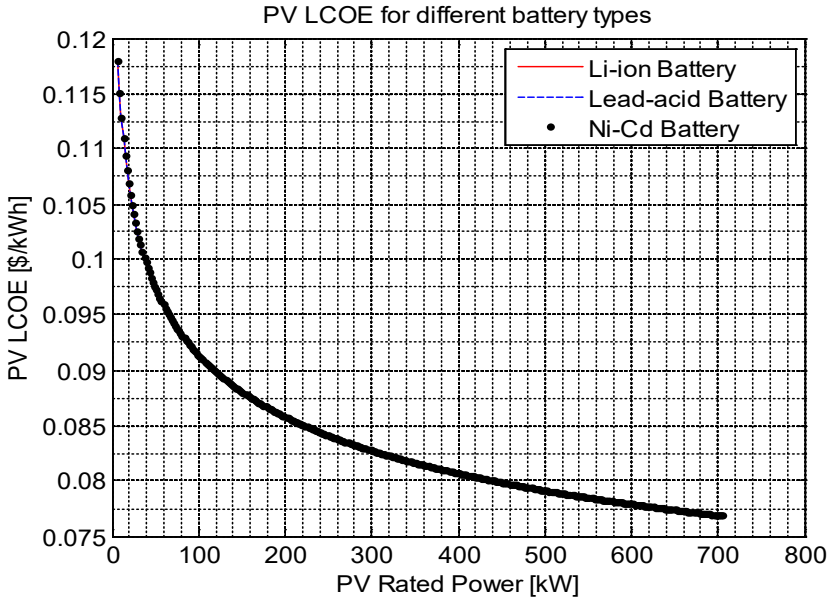

Figure 11. LCOE PV with 3 BESS

Table 7. LCOE for PV and 3 batteries

PV-BESS	$\mathbf{LCOE_{SYS}}$ [USD/kWh]
PV-LI-Ion	0.2379
PV- LEAD	0.3406
PV- Ni-Cd	0.2717

Table 8. LCOS for 3 batteries

Battery Type	Cost (USD/kWh)
Li-Ion	1.8594
Lead–Acid	6.1899
Ni-Cd	2.9153

Figure 12 displays the fuel cell's power output over all periods. As you can see, it does not always generate power. Instead, it produces power in short, large collapses, reaching a maximum of 113.16 kW. This indicates that the fuel cell only activates and runs when the system requires additional power. It serves as a very useful backup power source for various seasons of the year, providing power when other sources are insufficient or low.

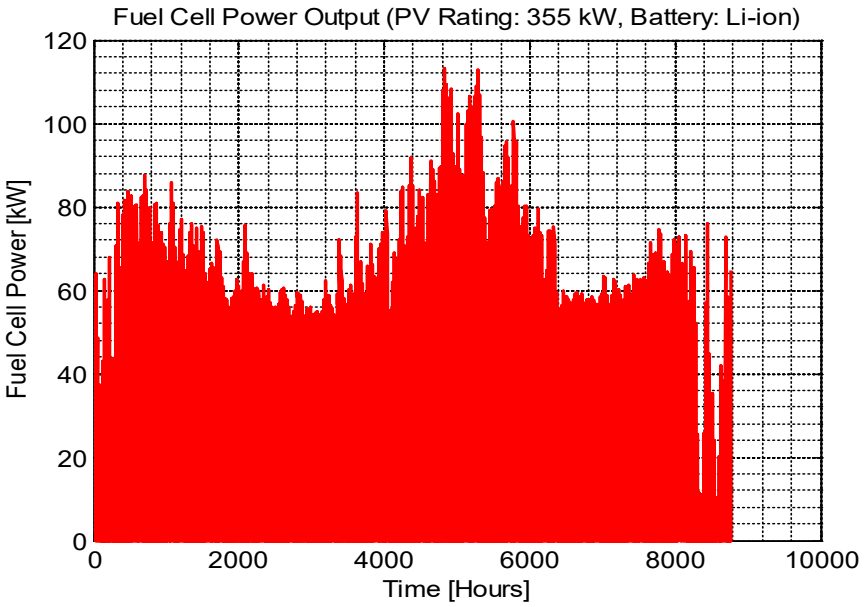

Figure 12. FC power produced

Figure 13 displays the electrolysis's power consumption over the period. It does not always use power, but when it does, it uses a lot. Its maximum power consumption is 301.57 kW. During its 1209 hours of operation, the electrolysis uses 169094.69 kWh in total. This demonstrates that the main objective is to consume additional power for extended periods of time, particularly whenever that power becomes available.

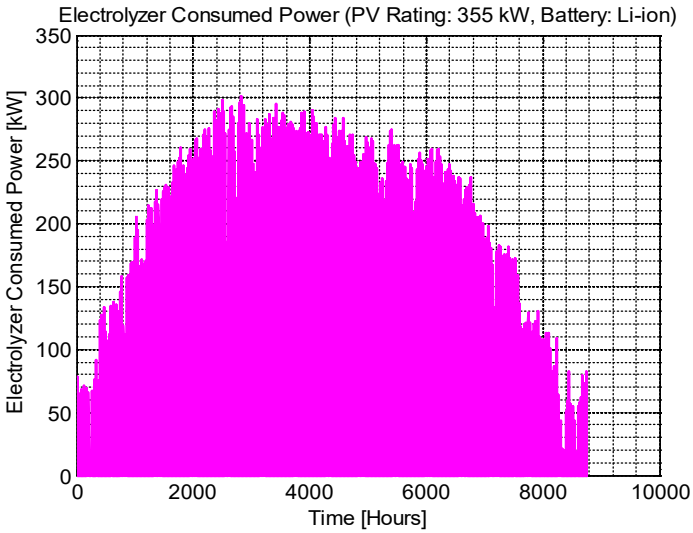

Figure 13. Electrolysis power consumption

Figure 14 shows that hydrogen tank's state of charge (SOC) over the period. The tank's operating range is 123.88 kWh, which is also its initial state of charge, and 619.38 kWh, which is its maximum capacity. According to the graph, the tank spends 2859 hours at or close to its lowest level throughout the period, while reaching or remaining close to its full capacity for 2571 hours. This pattern shows how well the tank manages energy fluctuations in the system by storing excess energy (as hydrogen) when it is available and releasing it when needed.

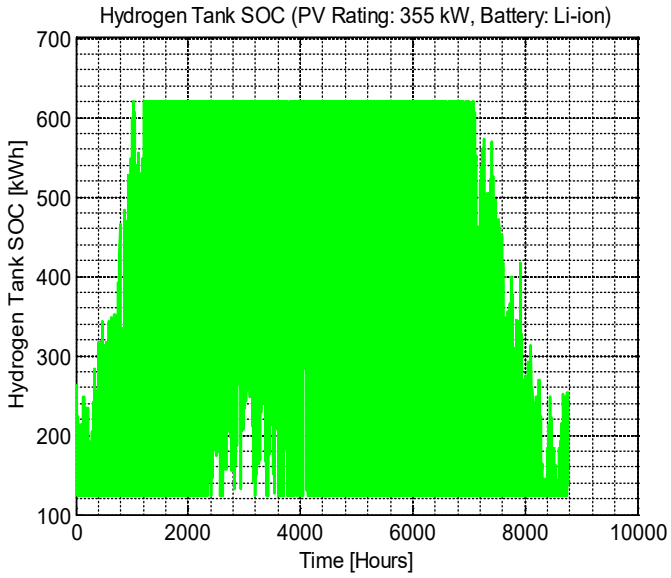

Figure 14. Hydrogen tank state of charge

Table 9 clearly shows that, once launch mass and transportation cost are taken into account, the battery bank becomes the dominant driver of logistics for the proposed lunar microgrid, and the choice of chemistry is therefore critical. For the same 2.5 MWh nominal capacity, the Ni-Cd and lead-acid options are approximately three and five times heavier than the Li-Ion pack, respectively, which inflates their launch cost from 1.5 × 108 USD for Li-Ion to 4.5 × 108 and 7.7 × 108 USD. Expressed per unit of stored energy, this means that transporting lead-acid storage to the lunar surface would cost on the order of 3.1 × 105 USD/kWh, more than five times the 6.0 × 104 USD/kWh associated with Li-Ion. In contrast, the PV array and hydrogen tank system each contribute less than half a tonne to the launch mass, with total transportation

costs of about 5 × 106 and 4.6 × 106 USD, respectively – almost two orders of magnitude lower than any of the battery options. The hydrogen system in particular combines a relatively low mass (0.43 t) with a high system-level specific energy, leading to a transportation cost intensity of only 7.5 × 103 USD/kWh, roughly eight times lower than the Li-Ion BESS. Taken together, these results indicate that (i) heavy chemistries such as lead-acid and Ni-Cd are effectively non-competitive for lunar applications, irrespective of their lower capital cost on Earth; (ii) Li-ion remains the only viable electrochemical option when launch cost is considered, reinforcing the LCOE-based conclusion of the techno-economic analysis; and (iii) space-oriented designs should minimise battery capacity and rely more heavily on high-specific-power PV arrays and hydrogen-based long-term storage, since these subsystems deliver substantial energy services at a comparatively modest mass and transportation cost.

From an environmental perspective, operation in high vacuum, intense radiation, and severe thermal cycling between long sunlit and eclipse periods constrains the selection and derating of PV modules, electrochemical storage, and power electronics, while pervasive abrasive dust (regolith) affects the expected degradation and maintenance requirements of exposed components. Operationally, the microgrid must support long-duration, crewed missions with limited on-site maintenance, restricted opportunities for hardware replacement, and strict reliability requirements, since even short interruptions to critical loads can compromise mission safety. These factors, together with the very high transport mass/cost of hardware delivery to the lunar surface, favour architectures with a small number of robust subsystems, minimal moving parts, simple supervisory control, and technologies with high specific power and energy. In this context, the optimised PV–Li-Ion–H2 configuration is not only cost-effective in LCOE and launch-mass terms, but also aligns with the need for high reliability, reduced maintenance interventions, and environmentally robust operation under the unique conditions of a lunar base.

Table 9. Mass and transportation cost estimation

Subsystem	Design basis	Mass[t]	Launch cost [USD]	Cost intensity*
Li-Ion BESS	2.5 MWh	13.9	1.50×10^8	6.0×10^4 USD/kWh
Ni-Cd BESS	2.5 MWh	41.7	4.50×10^8	1.8×10^5 USD/kWh
Lead-acid BESS	2.5 MWh	71.4	7.71×10^8	3.1×10^5 USD/kWh
PV array	70 kW	0.47	5.04×10^6	7.2×10^4 USD/kW
H_2 tank system	619 kWh (chemical)	0.43	4.62×10^6	7.5×10^3 USD/kWh

Validation

A complete energy balance analysis was used to evaluate the validity and dependability of the suggested hybrid energy system model PV, batteries, FC, and electrolysis. The purpose of this analysis was to verify that all energy flows in the system are exactly computed and checked during the simulation. The structure of the model built based on energy conservation is determined for each hourly time step and for the full simulation period (one year): using the following formula:

$$E_{\mathrm{PV}}{+}E_{\mathrm{B,dch}} + E_{\mathrm{FC}} + E_{\mathrm{UL}} = E_{\mathrm{L}} + E_{\mathrm{B,ch}} + E_{\mathrm{EL}} + E_{\mathrm{Excess}} \quad (40)$$

or

$$E_{\mathrm{PV}}{+}E_{\mathrm{B,dch}} + E_{\mathrm{FC}} + E_{\mathrm{UL}} - E_{\mathrm{L}} + E_{\mathrm{B,ch}} + E_{\mathrm{EL}} + E_{\mathrm{Excess}} \approx 0 \quad (41)$$

where are: E_{PV} - energy generated by PV system, $E_{\mathrm{B,dch}}$ - energy discharged from BESS, E_{FC} - energy output FC, E_{UL} - unserved load representing the unmet demand for energy, its inclusion on the sources side ensures that any energy deficit is accounted for in the overall balance, E_{L} - load demand, $E_{\mathrm{B,ch}}$ - energy charged into BESS, E_{EL} –energy consumed by the electrolysis for hydrogen production, E_{Excess} - representing excess energy produced that could not be used or stored. The overall energy balance at all times displayed a very slight variation, almost zero, after the simulation was run for a year for different system configurations. For example, the final energy balance difference was around -3.26×10^{-9} kWh. This minimal difference validates the simulation model's dependability and efficiency. It shows that every energy flow is carefully monitored and recorded, including production, consumption, storage, surplus, and deficit. The result strongly supports that the model accurately represents how the proposed hybrid system works and makes sensible, balanced predictions about energy flows, which enhances the reliability of the technical and economic assessments based on it, all this is illustrated in the next table, **Table 10**.

This energy-balance check is used as a numerical validation of the proposed hybrid system model. Since the entire PV–BESS–FC–electrolyser–H_2 model is formulated on the basis of energy conservation, the very small residual obtained over the full year (on the order of 10^{-9} kWh) confirms that all energy flows are consistently accounted for in the simulation. In other words, the implementation correctly tracks production, storage, consumption, curtailed energy and unserved load at every time step, and no artificial gain or loss of energy is introduced by the numerical model. As the study concerns a prospective lunar microgrid for which full-scale experimental data are not yet available, this internal energy-balance verification provides a practical way to ensure that the technical and economic results are built on a physically consistent representation of the system.

Table 10. Energy flow summary

Energy Parameter	Value in kWh
Total PV Generation	801219.86
Total Battery Discharge	176071.48
Total Fuel Cell Output	93417.06
Total Energy Generated	1070708.40
Total Load Consumed	663841.93
Total Battery Charge	191382.05
Total Electrolysis Consumption	169094.69
Total Energy Consumed	1024318.66
Total Curtailed Energy	139294.30
Total Unserved Load	92904.55
Overall Energy Balance Check	$-3.26 * 10^{-9}$

CONCLUSION AND FUTURE WORK

This study presented a comprehensive techno-economic assessment and optimal design framework for a hybrid renewable energy system tailored for space microgrid applications, with specific emphasis on lunar surface power supply. By integrating photovoltaic generation with a battery energy storage system (BESS) and a hydrogen-based storage subsystem comprising an electrolyser, hydrogen tank, and fuel cell, the proposed system demonstrates high reliability and competitiveness under the stringent constraints of extraterrestrial environments. An enhanced LCOE formulation, coupled with hourly simulations of load

demand and system operation, enabled accurate sizing of the PV–BESS–FC architecture and provided a realistic estimate of lifecycle performance. Results confirm that the proposed hybrid system can supply the annual electrical load of the reference lunar base with negligible unserved energy, achieving a levelized cost of electricity of 0.2379 USD/kWh. Among the evaluated technologies, lithium-ion batteries proved to be the most cost-effective and technically suitable option for short-term storage, offering the lowest LCOS, system-level LCOE, and launch-related transportation cost. In contrast, lead–acid and Ni–Cd batteries were shown to be impractical due to their low specific energy and excessive transport mass.

Meanwhile, the hydrogen subsystem demonstrated strong potential for medium- and long-duration autonomy, particularly during extended lunar eclipse periods, enabling the battery bank to be sized for short-term balancing rather than full-duration backup. The findings also highlight that technology preferences commonly derived from terrestrial microgrid applications cannot be directly transferred to space environments. Constraints such as launch mass, transportation cost, and surface operational reliability necessitate prioritising high-specific-power PV technologies, lithium-ion BESS, and hydrogen-based long-term storage solutions. The modelling framework and results presented in this study provide valuable design guidelines for future space missions, supporting the development of sustainable, resilient, and economically viable energy systems for lunar and deep-space habitats. Future work may explore the effects of component degradation, lunar dust accumulation on PV modules, extreme thermal cycles, radiation-induced performance shifts, and advanced power management algorithms. Moreover, incorporating alternative storage technologies or emerging space-qualified materials could enhance the durability and efficiency of next-generation space microgrids.

Limitations and Future Work

The present analysis is restricted to a single reference configuration with preselected component capacities and uses simplified models for thermal control, degradation and reliability. The mass and transportation-cost estimates are based on representative specific-energy values and average cost per kilogram to the lunar surface, rather than on a detailed structural design. In addition, the load profile does not yet include fully dynamic in-situ resource utilisation (ISRU) processes, which can introduce large, variable industrial loads. Future work should therefore extend the framework in several directions:

(i) perform a full multi-objective optimisation that jointly minimises LCOE and launch mass while enforcing strict reliability constraints;
(ii) integrate time-varying ISRU loads (e.g. oxygen and propellant production) to quantify their impact on optimal sizing and operation;
(iii) incorporate more detailed thermal, degradation and reliability models for components operating in the lunar environment; and
(iv) explore alternative generation and storage options within the same mass-aware framework.

These developments will further refine the design of cost-effective, mass-efficient hybrid microgrids for future lunar and deep-space missions.

REFERENCES

1. Saha, D., Bazmohammadi, N., Raya-Armenta, J. M., Bintoudi, A. D., Lashab, A., Vasquez, J. C. and Guerrero, J. M., Optimal Sizing and Siting of PV and Battery Based Space Microgrids Near the Moon's Shackleton Crater, *IEEE Access*, Vol. 11, pp 8701–8717, 2023, https://doi.org/10.1109/ACCESS.2023.3239303.
2. Sherwood, B., Principles for a Practical Moon Base, *Acta Astronautica*, Vol. 160, pp 116–124, 2019, https://doi.org/10.1016/j.actaastro.2019.04.018.

3. Chavy-Macdonald, M.-A., Oizumi, K., Kneib, J.-P. and Aoyama, K., The cis-lunar ecosystem — A systems model and scenarios of the resource industry and its impact, *Acta Astronautica*, Vol. 188, pp 545–558, 2021, https://doi.org/10.1016/j.actaastro.2021.06.017.
4. Del Canto Viterale, F., Transitioning to a New Space Age in the 21st Century: A Systemic-Level Approach, *Systems*, Vol. 11, No. 5, Art. 232, 2023, https://doi.org/10.3390/systems11050232.
5. Saha, D., Bazmohammadi, N., Raya-Armenta, J. M., Bintoudi, A. D., Lashab, A., Vasquez, J. C. and Guerrero, J. M., Space Microgrids for Future Manned Lunar Bases: A Review, *IEEE Open Access Journal of Power and Energy*, Vol. 8, pp 570–583, 2021, https://doi.org/10.1109/OAJPE.2021.3116674.
6. Colozza, A. J., *Small Lunar Base Camp and In Situ Resource Utilization Oxygen Production Facility Power System Comparison*, (Technical) Report NASA/CR—2020-220368, National Aeronautics and Space Administration (NASA), Glenn Research Center, Cleveland, Ohio, USA, 2020.
7. Fincannon, H. J., Lunar Environment and Lunar Power Needs, in: Springer Handbook of Space Engineering, Springer Nature, Cham, Switzerland, 2020.
8. Soeder, J. F., Dever, T. P., McNelis, A. M., Beach, R. F., Trase, L. M. and May, R. D., Overview of Intelligent Power Controller Development for Human Deep Space Exploration, *Proceedings of the 12th International Energy Conversion Engineering Conference* (American Institute of Aeronautics and Astronautics (AIAA)), Cleveland, Ohio, USA, 28–30 July 2014, https://doi.org/10.2514/6.2014-3833.
9. Bintoudi, A. D., Timplalexis, C., Mendes, G., Guerrero, J. M. and Demoulias, C., *Design of Space Microgrid for Manned Lunar Base: Spinning-in Terrestrial Technologies*, Proceedings of the European Space Power Conference (ESPC) (European Space Agency (ESA)), Juan-les-Pins, France, 30 September–4 October 2019, pp. 1–8, https://doi.org/10.1109/ESPC.2019.8932024.
10. Choi, S. H., King, G. C., Kim, H.-J. and Park, Y., Electrostatic Power Generation from Negatively Charged, Simulated Lunar Regolith, Proceedings of the AIAA SPACE Conference and Exposition (American Institute of Aeronautics and Astronautics (AIAA)), Anaheim, California, USA, 31 August–2 September 2010.
11. Gilbert, A. Q., Astronaut Nuclear Safety: A Concept for Managing Crew Risks When Using Space Nuclear Power Systems, *Journal of Space Safety Engineering*, Vol. 12, No. 2, pp 266–273, 2025, https://doi.org/10.1016/j.jsse.2025.04.009.
12. Gietl, E. B., Gholdston, E. W., Manners, B. A. and Delventhal, R. A., *The Electric Power System of the International Space Station — A Platform for Power Technology Development*, Proceedings of the IEEE Aerospace Conference (Institute of Electrical and Electronics Engineers (IEEE)), Big Sky, Montana, USA, 18–25 March 2000, Vol. 4, pp. 47–54, https://doi.org/10.1109/AERO.2000.878364.
13. Pappa, R., Taylor, C., Warren, J., Chamberlain, M., Cook, S., Belbin, S., Lepsch, R., Tiffin, D., Doggett, B., Mikulas, M., Wong, I., Long, D., Steinkoening, D., Pensado, A., Blandino, J. and Haste, J., Relocatable 10 kW Solar Array for Lunar South Pole Missions, (Technical) Report, National Aeronautics and Space Administration (NASA), Langley Research Center, Hampton, Virginia, USA, NASA/TM-20210011743, 2021.
14. Ali, A. O., Elgohr, A. T., El-Mahdy, M. H., Zohir, H. M., Emam, A. Z., Mostafa, M. G., Al-Razgan, M., Kasem, H. M. and Elhadidy, M. S., Advancements in Photovoltaic Technology: A Comprehensive Review of Recent Advances and Future Prospects, *Energy Conversion and Management: X*, Vol. 26, Art. 100952, 2025, https://doi.org/10.1016/j.ecmx.2025.100952.
15. Hassan, M. A., Eladl, A. A., Sedhom, B. E. and Saeed, M. A., A New Optimal Centralized Demand Side Management for a Campus Smart Microgrid, *Proceedings of the 32nd International Symposium on Industrial Electronics* (Institute of Electrical and Electronics

Engineers (IEEE)), Helsinki, Finland, 19–21 June 2023, pp 1–6, https://doi.org/10.1109/ISIE51358.2023.10228127.
16. Freeh, J., Analysis of Stationary, Photovoltaic-Based Surface Power System Designs at the Lunar South Pole, *Proceedings of the AIAA SPACE Conference and Exposition* (American Institute of Aeronautics and Astronautics (AIAA)), San Diego, California, USA, 9–11 September 2008, https://doi.org/10.2514/6.2008-7810.
17. Lopez, F., Mauro, A., Mauro, S., Monteleone, G., Sfasciamuro, D. E. and Villa, A., *A Lunar-Orbiting Satellite Constellation for Wireless Energy Supply*, Aerospace, Vol. 10, No. 11, Art. 919, 2023, https://doi.org/10.3390/aerospace10110919.
18. MacAlpine, S. and Deline, C., Modeling Microinverters and DC Power Optimizers in PVWatts, (Technical) Report, National Renewable Energy Laboratory (NREL), Golden, Colorado, USA, NREL/TP-5J00-63463, 2015, https://doi.org/10.2172/1171792, [Accessed: Dec. 20, 2025].
19. Guzik, M. C., Jakupca, I., Gilligan, R., Bennett, W. R., Smith, P. J. and Fincannon, J., Regenerative Fuel Cell Power Systems for Lunar and Martian Surface Exploration, *Proceedings of the AIAA SPACE and Astronautics Forum and Exposition* (American Institute of Aeronautics and Astronautics (AIAA)), Orlando, Florida, USA, 12–14 September 2017, https://doi.org/10.2514/6.2017-5368.
20. Lashab, A., Yaqoob, M., Terriche, Y., Vasquez, J. C. and Guerrero, J. M., Space Microgrids: New Concepts on Electric Power Systems for Satellites, *IEEE Electrification Magazine*, Vol. 8, No. 4, pp 8–19, 2020, https://doi.org/10.1109/MELE.2020.3032866.
21. Zakaria, A., Eladl, A. A., Mansy, I. I. and Abdelkader, S. M., *Sizing PV-Battery Storage Grid-Connected System Based on Levelized Cost of Energy*, Proceedings of the *International Middle East Power System Conference (MEPCON)*, Cairo, Egypt, 19–21 December 2023, pp 1–7.
22. Fincannon, J., Characterization of Lunar Polar Illumination from a Power System Perspective, *Proceedings of the 46th AIAA Aerospace Sciences Meeting and Exhibit* (American Institute of Aeronautics and Astronautics (AIAA)), Reno, Nevada, USA, 7–10 January 2008.
23. Khan, Z., Vranis, A., Zavoico, A., Freid, S. and Manners, B., Power System Concepts for the Lunar Outpost: A Review of the Power Generation, Energy Storage, Power Management and Distribution (PMAD) System Requirements and Potential Technologies, *AIP Conference Proceedings*, Vol. 813, No. 1, pp 1083–1092, 2006, https://doi.org/10.1063/1.2169241.
24. Fincannon, J., Lunar South Pole Illumination: Review, Reassessment, and Power System Implications, *Proceedings of the Fifth International Energy Conversion Engineering Conference and Exhibit* (American Institute of Aeronautics and Astronautics (AIAA)), St. Louis, Missouri, USA, 25–28 June 2007.
25. Dhar, P., Engineers Are Working on a Solar Microgrid to Outlast Lunar Nights, *IEEE Spectrum*, Online article, 2022, https://spectrum.ieee.org/lunar-solar-microgrid, [Accessed: Aug. 18, 2024].
26. Tamponnet, C., Life Support Systems for Lunar Missions, *Advances in Space Research*, Vol. 18, No. 11, pp 103–110, 1996, https://doi.org/10.1016/0273-1177(96)00096-8.
27. Oberst, J., Christou, A., Suggs, R., Moser, D., Daubar, I. J., McEwen, A. S., Burchell, M. J., Kawamura, T., Hiesinger, H., Wünnemann, K., Wagner, R. and Robinson, M. S., The Present-Day Flux of Large Meteoroids on the Lunar Surface — A Synthesis of Models and Observational Techniques, *Planetary and Space Science*, Vol. 74, No. 1, pp 179–193, 2012, https://doi.org/10.1016/j.pss.2012.10.005.
28. Benaroya, H., Reliability and Damage, in: *Building Habitats on the Moon: Engineering Approaches to Lunar Settlements* (Benaroya, H., ed.), Springer International Publishing, Cham, Switzerland, pp 249–285, 2018, https://doi.org/10.1007/978-3-319-68243-3_9.

29. Schonberg, W. P., Schäfer, F. and Putzar, R., Some Comments on the Protection of Lunar Habitats against Damage from Meteoroid Impacts, *Journal of Aerospace Engineering*, Vol. 23, No. 1, pp 90–97, 2010, https://doi.org/10.1061/(ASCE)0893-1321(2010)23:1(90).
30. Barker, M. K., Mazarico, E., Neumann, G. A., Smith, D. E., Zuber, M. T. and Head, J. W., Improved LOLA Elevation Maps for South Pole Landing Sites: Error Estimates and Their Impact on Illumination Conditions, *Planetary and Space Science*, Vol. 203, Art. 105119, 2021, https://doi.org/10.1016/j.pss.2020.105119.
31. Leone, G., Ahrens, C., Korteniemi, J., Gasparri, D., Kereszturi, A., Martynov, A., Schmidt, G. W., Calabrese, G. and Joutsenvaara, J., Sverdrup-Henson Crater: A Candidate Location for the First Lunar South Pole Settlement, *iScience*, Vol. 26, No. 10, Art. 107853, 2023, https://doi.org/10.1016/j.isci.2023.107853.
32. Carbone, M., Sajadi, A. and Loparo, K., Bifurcation Analysis of DC Electric Power Systems for Deep Space Exploration Spacecraft, *Proceedings of the IEEE Power and Energy Conference at Illinois (PECI)* (Institute of Electrical and Electronics Engineers (IEEE)), Champaign, Illinois, USA, 28 February–1 March 2019, pp 1–7.
33. Hu, G., Chen, K., Huang, Q., Guo, W., Li, Q., Gui, L. and Cheng, Y., Brightness Temperature Calculation of Lunar Crater: Interpretation of Topographic Effect on Microwave Data from Chang'E, *IEEE Transactions on Geoscience and Remote Sensing*, Vol. 52, No. 8, pp 4499–4510, 2014, https://doi.org/10.1109/TGRS.2013.2282342.
34. Hu, G. P., Zheng, Y. C., Xu, A. A. and Tang, Z. S., Lunar Surface Temperature of Global Moon: Preparation of Database with Topographic and Albedo Effects, *IEEE Geoscience and Remote Sensing Letters*, Vol. 13, No. 1, pp 110–114, 2016, https://doi.org/10.1109/LGRS.2015.2499305.
35. Hurley, D. M., Sarantos, M., Grava, C., Williams, J. P., Retherford, K. D., Siegler, M., Greenhagen, B. and Paige, D., An Analytic Function of Lunar Surface Temperature for Exospheric Modeling, *Icarus*, Vol. 255, pp 159–163, 2015, https://doi.org/10.1016/j.icarus.2014.08.043.
36. Ciurans, C., Bazmohammadi, N., Vasquez, J. C., Dussap, G., Guerrero, J. M. and Godia, F., Hierarchical Control of Space Closed Ecosystems: Expanding Microgrid Concepts to Bioastronautics, *IEEE Industrial Electronics Magazine*, Vol. 15, No. 2, pp 16–27, 2021, https://doi.org/10.1109/MIE.2020.3026828.
37. Colozza, A., Heller, R., Wong, W. and Hepp, A., Solar Energy Systems for Lunar Oxygen Generation, Proceedings of the 48th AIAA Aerospace Sciences Meeting Including the New Horizons Forum and Aerospace Exposition (American Institute of Aeronautics and Astronautics (AIAA)), Orlando, Florida, USA, 4–7 January 2010.
38. Nakamura, T. and Smith, B., Solar Power System for Lunar ISRU Applications, Proceedings of the 48th AIAA Aerospace Sciences Meeting Including the New Horizons Forum and Aerospace Exposition (American Institute of Aeronautics and Astronautics (AIAA)), Orlando, Florida, USA, 4–7 January 2010.
39. Gordon, P. E. C., Colozza, A. J., Hepp, A. F., Heller, R. S., Gustafson, R. J., Stern, T. G. and Nakamura, T., *Thermal Energy Process Heat for Lunar ISRU: Technical Challenges and Technology Opportunities*, Proceedings of the *49th AIAA Aerospace Sciences Meeting Including the New Horizons Forum and Aerospace Exposition* (American Institute of Aeronautics and Astronautics (AIAA)), Orlando, Florida, USA, 4–7 January 2011.
40. Cataldo, R. L. and Bozek, J. M., Power Requirements for the First Lunar Outpost, *AIP Conference Proceedings*, Vol. 271, No. 1, pp 1–9, 1993, https://doi.org/10.1063/1.43249.
41. Kerslake, T. W., Electric Power System Technology Options for Lunar Surface Missions, (Technical) Report, National Aeronautics and Space Administration (NASA), Glenn Research Center, Cleveland, Ohio, USA, NASA/TM-2005-213629, 2005.
42. Paulsen, G., Zacny, K., Kim, D., Mank, Z., Wang, A., Thomas, T., Hyman, C., Mellerowicz, B., Yaggi, B., Fitzgerald, Z., Ridilla, A., Atkinson, J., Quinn, J., Smith, J.

and Kleinhenz, J., TRL6 Lunar Resource Prospector Drill, Poster Abstract, *48th Annual Lunar and Planetary Science Conference*, The Woodlands, Texas, USA, 20–24 March 2017.

43. Csank, J. and Scott, J. H., Power and Energy for the Lunar Surface, Presentation, Advanced Research Projects Agency–Energy (ARPA-E), Tech-to-Market Team, Virtual, 29 April 2022.
44. Fernandez Lisbona, E., IV-3 – Calibration, Testing and Monitoring of Space Solar Cells, in: *Practical Handbook of Photovoltaics* (Markvart, T. and Castañer, L., eds.), Elsevier Science, Amsterdam, The Netherlands, pp 825–853, 2003.
45. Zhao, X. F., Aierken, A., Heini, M., Tan, M., Wu, Y. Y., Lu, S. L. et al., Degradation Characteristics of Electron and Proton Irradiated InGaAsP/InGaAs Dual Junction Solar Cell, *Solar Energy Materials and Solar Cells*, Vol. 206, Art. 110339, 2020, https://doi.org/10.1016/j.solmat.2019.110339.
46. Kaya, A., Tok, M. E. and Koc, M., A Levelized Cost Analysis for Solar-Energy-Powered Sea Water Desalination in the Emirate of Abu Dhabi, *Sustainability*, Vol. 11, No. 6, 2019, https://doi.org/10.3390/su11061691.
47. Ferreira, A., Kunh, S. S., Fagnani, K. C., de Souza, T. A., Tonezer, C., dos Santos, G. R. and Coimbra Araújo, C. H., Economic Overview of the Use and Production of Photovoltaic Solar Energy in Brazil, *Renewable and Sustainable Energy Reviews*, Vol. 81, pp 181–191, 2018, https://doi.org/10.1016/j.rser.2017.06.102.
48. Obi, M., Jensen, S. M., Ferris, J. B. and Bass, R. B., Calculation of Levelized Costs of Electricity for Various Electrical Energy Storage Systems, *Renewable and Sustainable Energy Reviews*, Vol. 67, pp 908–920, 2017, https://doi.org/10.1016/j.rser.2016.09.043.
49. Jones, H. W., *Take Material to Space or Make It There?*, Proceedings of *ASCEND 2023* (American Institute of Aeronautics and Astronautics (AIAA)), Las Vegas, Nevada, USA, 23–25 October 2023, https://doi.org/10.2514/6.2023-4618.
50. Khan, F. M. N. U., Rasul, M. G., Sayem, A. S. M. and Mandal, N., Maximizing Energy Density of Lithium-Ion Batteries for Electric Vehicles: A Critical Review, *Energy Reports*, Vol. 9, pp 11–21, 2023, https://doi.org/10.1016/j.egyr.2023.08.069
51. Eftekhari, A., Lithium Batteries for Electric Vehicles: From Economy to Research Strategy, *ACS Sustainable Chemistry & Engineering*, Vol. 7, No. 6, pp 5602–5613, 2019, https://doi.org/10.1021/acssuschemeng.8b01494.
52. Battlebury, D. R., A High-Performance Lead–Acid Battery for EV Applications, *Journal of Power Sources*, Vol. 80, No. 1, pp 7–11, 1999, https://doi.org/10.1016/S0378-7753(98)00247-X.
53. Posada, J. O. G., Rennie, A. J. R., Villar, S. P., Martins, V. L., Marinaccio, J., Barnes, A., Glover, C. F. and Worsley, D. A., Aqueous Batteries as Grid-Scale Energy Storage Solutions, *Renewable and Sustainable Energy Reviews*, Vol. 68, pp 1174–1182, 2017, https://doi.org/10.1016/j.rser.2016.02.024.
54. Omar, N., Firouz, Y., Monem, M. A., Samba, A., Gualous, H., Coosemans, T., Van den Bossche, P. and Van Mierlo, J., Analysis of Nickel-Based Battery Technologies for Hybrid and Electric Vehicles, in: *Reference Module in Chemistry, Molecular Sciences and Chemical Engineering*, Elsevier, 2014, https://doi.org/10.1016/B978-0-12-409547-2.10740-1.
55. Law, D. C., Edmondson, K. M., Siddiqi, N., Paredes, A., King, R. R., Glenn, G., Lebois, E., Haddad, M. H., Isshiki, T. D. and Karam, N. H., Lightweight, Flexible, High-Efficiency III-V Multijunction Cells, *Proceedings of the 4th World Conference on Photovoltaic Energy Conversion* (Institute of Electrical and Electronics Engineers (IEEE)), Waikoloa, Hawaii, USA, 7–12 May 2006, Vol. 2, pp 1879–1882, https://doi.org/10.1109/WCPEC.2006.279862.
56. Mikulas, M. M., Pappa, R. S., Warren, J. and Rose, G., Telescoping Solar Array Concept for Achieving High Packaging Efficiency, *Proceedings of the AIAA Spacecraft Structures*

Conference (American Institute of Aeronautics and Astronautics (AIAA)), Kissimmee, Florida, USA, 5–9 January 2015.
57. Pappa, R. S., Rose, G., Chamberlain, M. K., Paddock, D. and Mikulas, M., Compact Telescoping Surface Array for Mars Solar Power, *Proceedings of the AIAA Spacecraft Structures Conference* (American Institute of Aeronautics and Astronautics (AIAA)), Kissimmee, Florida, USA, 8–12 January 2018.
58. Noussan, M., Raimondi, P. P., Scita, R. and Hafner, M., The Role of Green and Blue Hydrogen in the Energy Transition — A Technological and Geopolitical Perspective, *Sustainability*, Vol. 13, No. 1, 2021, https://doi.org/10.3390/su13010298.
59. Hua, T. Q., Roh, H.-S. and Ahluwalia, R. K., Performance Assessment of 700-bar Compressed Hydrogen Storage for Light-Duty Fuel Cell Vehicles, *International Journal of Hydrogen Energy*, Vol. 42, No. 40, pp 25121–25129, 2017, https://doi.org/10.1016/j.ijhydene.2017.08.123.
60. Bortolini, M., Gamberi, M. and Graziani, A., Technical and Economic Design of Photovoltaic and Battery Energy Storage System, *Energy Conversion and Management*, Vol. 86, pp 81–92, 2014, https://doi.org/10.1016/j.enconman.2014.04.089.
61. Elnozahy, A., Yousef, A. M., Ghoneim, S. S. M., Abdelwahab, S. A. M., Mohamed, M. and Abo-Elyousr, F. K., *Optimal Economic and Environmental Indices for Hybrid PV/Wind-Based Battery Storage System*, Journal of Electrical Engineering & Technology, Vol. 16, No. 6, pp 2847–2862, 2021, https://doi.org/10.1007/s42835-021-00810-9.
62. Luo, X., Wang, J., Dooner, M. and Clarke, J., Overview of Current Development in Electrical Energy Storage Technologies and the Application Potential in Power System Operation, *Applied Energy*, Vol. 137, pp 511–536, 2015, https://doi.org/10.1016/j.apenergy.2014.09.081.
63. Kamarudin, S. K., Daud, W. R. W., Md Som, A., Takriff, M. S. and Mohammad, A. W., Technical Design and Economic Evaluation of a PEM Fuel Cell System, *Journal of Power Sources*, Vol. 157, No. 2, pp 641–649, 2006, https://doi.org/10.1016/j.jpowsour.2005.10.053.
64. de Bruijn, F. A., Dam, V. A. T. and Janssen, G. J. M., Review: Durability and Degradation Issues of PEM Fuel Cell Components, *Fuel Cells*, Vol. 8, No. 1, pp 3–22, 2008, https://doi.org/10.1002/fuce.200700053.
65. Murdoch, H., Munster, J., Satyapal, S., Rustagi, N., Elgowainy, A. and Penev, M., Pathways to Commercial Liftoff: Clean Hydrogen, (Technical) Report, U.S. Department of Energy, Washington, D.C., USA, 2023.
66. Burke, A., Ogden, J., Fulton, L. and Cerniauskas, S., Hydrogen Storage and Transport: Technologies and Costs, (Technical) Report, Institute of Transportation Studies, University of California, Davis, California, USA, 2024.

Paper submitted: 22.08.2025
Paper revised: 24.12.2025
Paper accepted: 07.01.2026